A Critical Review of the Li Insertion Mechanisms in LiFePO[subscript 4] Electrodes

Citation: Malik, R., A. Abdellahi, and G. Ceder. "A Critical Review of the Li Insertion Mechanisms in LiFePO4 Electrodes." Journal of the Electrochemical Society 160, no. 5 (January 1, 2013): A3179–A3197. © 2013 The Electrochemical Society

As Published: http://dx.doi.org/10.1149/2.029305jes

Publisher: Electrochemical Society

Persistent URL: http://hdl.handle.net/1721.1/91661

Version: Final published version: final published article, as it appeared in a journal, conference proceedings, or other formally published context

Journal of The Electrochemical Society, **160** (5) A3179-A3197 (2013)
0013-4651/2013/160(5)/A3179/19/$31.00 © The Electrochemical Society

JES Focus Issue on Intercalation Compounds for Rechargeable Batteries

A Critical Review of the Li Insertion Mechanisms in $LiFePO_4$ Electrodes

Rahul Malik, Aziz Abdellahi, and Gerbrand Ceder[*,z]

Department of Materials Science, Massachusetts Institute of Technology, Cambridge, Massachusetts 02139, USA

With the ever-growing public and now commercial sentiment supporting the widespread adoption of low and zero-emission vehicles, it is unsurprising that Li-ion batteries which currently assume the bulk of the cost of electrified vehicles (a significant proportion coming from cost of battery materials) have become prolific not only in the primary research literature but have also entered the general public consciousness. Since the initial work in 1997, over 2000 research publications have been authored on lithium iron phosphate ($LiFePO_4$), one of only a handful of commercially viable Li-ion battery cathode materials currently used in electrified vehicles. Despite the sheer quantity of research devoted to the subject and the well-demonstrated excellent battery performance of $LiFePO_4$, what *is* surprising are the number of apparent discrepancies and ensuing contention in the literature regarding its (de)lithiation kinetics. This Review forgoes re-summarizing the well-accepted materials properties of $LiFePO_4$ and instead seeks to address headlong the specific areas of dispute in the field, specifically by considering how the thermodynamics and kinetics of Li intercalation are modified from the bulk to single-particle to multi-particle scales, shedding light on what makes $LiFePO_4$ such a unique material and ideally shaping future discourse of $LiFePO_4$ research.
 [DOI: 10.1149/2.029305jes]

Manuscript submitted February 1, 2013; revised manuscript received April 17, 2013. Published May 8, 2013. *This paper is part of the JES Focus Issue on Intercalation Compounds for Rechargeable Batteries*.

Most of the salient bulk properties of $LiFePO_4$ were characterized accurately in the very first $LiFePO_4$ papers[1] – open-circuit voltage (OCV; at ∼3.4 V vs. Li metal shown in Figure 1), ordered olivine crystal structure, reversible topotactic Li intercalation with theoretical capacity ∼170 mAh/g, room temperature Li phase separation, and both excellent stability and cycling ability. The now well-known excellent rate performance of the material, however, was demonstrated only in the years following, defying the initial claim that $LiFePO_4$ would be strictly relegated to low-rate applications because of kinetic barriers associated with propagating a two-phase interface within an active particle.[1] In fact, through a series of notable experimental modifications the rate performance has been steadily improved to the extent that $LiFePO_4$ is considered suitable for high-rate applications (power tools, electrified vehicles, power grid, etc.). These key improvements have come through a combination of the following: reducing the active particle size to the nano-scale,[2,3] coating active particles with carbon,[4] incorporating dopant impurities,[5] diluting the active mass within the electrode with electrochemically inactive material,[6] and coating active particles with glassy ionic conductors.[7] The question now strays from *can* $LiFePO_4$ be a high-rate battery material, to *why*? The first step toward answering this question and developing a complete picture of lithiation intercalation kinetics within a $LiFePO_4$ composite electrode lies in understanding the nuances of the Li_xFePO_4 ($0 < x < 1$) system equilibrium itself.

Li_xFePO_4 ($0 < x_{Li} < 1$) – Bulk, Single-Particle, and Many Particle Thermodynamics

Bulk thermodynamics

Perhaps the defining feature of the Li_xFePO_4 system is the strong room-temperature Li phase separation with negligible Li solubility in the end-member phases (heterosite and triphylite).[8] In accordance with Gibbs' phase rule, which stipulates that there can be zero degrees of freedom in the intensive variables in the two-phase regime of a two-component system (given fixed pressure and temperature), this gives rise to the characteristic flat room-temperature voltage curve ubiquitous in the literature, illustrated in Figure 1. Of all the commercially functioning Li battery cathode materials, $LiFePO_4$ is unique to having this property – $LiCoO_2$,[9] $LiMn_2O_4$,[10] $Li(Ni,Co,Al)O_2$, and $Li(Ni,Co,Mn)O_2$[11] all form solid solutions over a wide concentration range, and if present at all, first-order phase transitions are weak arising from either Li ordering[9] or electronic effects.[12]

Thorough experimental[13,14] and computational[15] characterizations of the bulk Li composition–temperature binary phase diagram (shown in Figure 2) reveal the existence of a solid-solution phase which emerges through a eutectoid transition (at ∼400–500 K, x_{Li} ∼0.4–0.6). The complex high T behavior of the system arises from the unique contribution of the electron configurational entropy which stabilizes the solid-solution phase. In a conventional binary 'miscibility gap'–type system, interactions between unlike species (i.e. Li and vacancy) are purely repulsive, which encourages like species to pool together, but in Li_xFePO_4 the presence of localized $3d$ electrons[15,16] (i.e. e^-/Fe^{2+} or h^+/Fe^{3+}) on the transition metal sub-lattice complicates matters. To accurately model the finite-temperature phase behavior of Li_xFePO_4, both the ionic and electronic degrees of freedom must be explicitly considered. At low temperatures (below the eutectoid point), strong attractive interactions between Li^+ and e^- (Fe^{2+}) overcome repulsive Li^+–Li^+ and e^-–e^- interactions, overall stabilizing the phase separated state. The e^- (Fe^{2+}) effectively acts as the "glue" between the Li^+

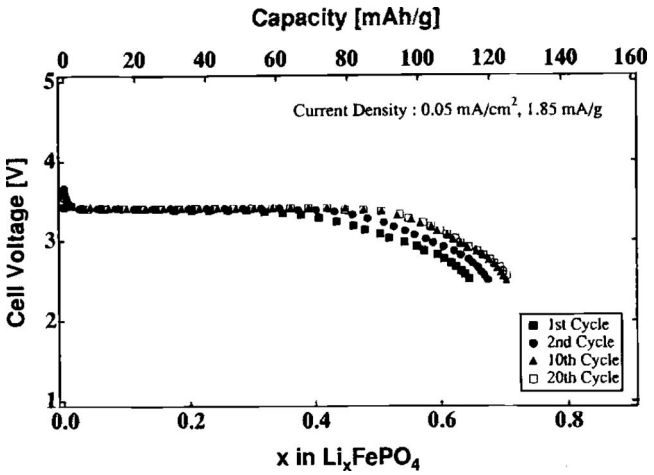

Figure 1. Discharge/charge curves vs. lithium at 2.0 mA/g (0.05 mA/cm^2) for Li_xFePO_4 obtained by Padhi et al.[1] Reprinted with permission from Ref. 1, copyright 1997, The Electrochemical Society.

*Electrochemical Society Active Member.
zE-mail: gceder@mit.edu

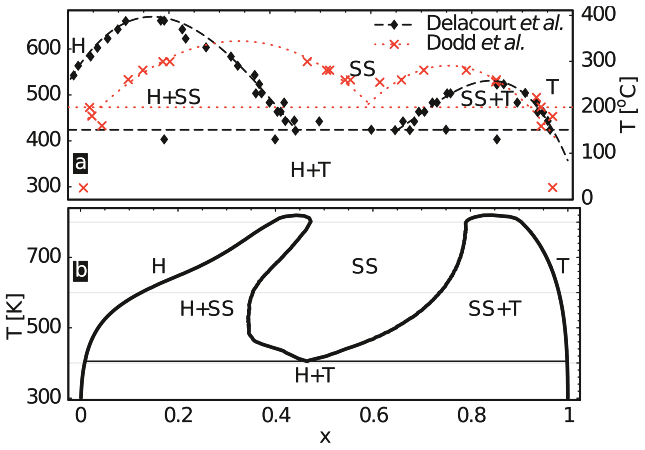

Figure 2. Bulk Li_xFePO_4 phase diagram as determined (a) experimentally by Dodd et al.[14] and Delacourt et al.[13] and (b) computationally by Zhou et al.[15] Reprinted with permission from Ref. 15, copyright 2006 by The American Physical Society.

ions. The combined effect of strong attractive Li^+–e^- interactions and the geometry of the olivine structure, which has twice as many nearest-neighbor Li^+–e^- pairs compared to repulsive Li^+–Li^+ pairs (the next strongest interaction as determined from first-principles calculations), not only favors phase-separation but also ensures that there is very little solubility in the coexisting phases. At higher temperatures above the eutectoid point, however, the increased configurational disorder of electrons and holes (Fe^{2+} and Fe^{3+}) prevents Li^+ from coalescing together into a separate phase, consequently diluting the number of attractive Li^+–e^- interactions and overall supporting solid solution formation.[15] This can be readily seen in experimental measurements of the Fe-site electron mobility with increasing temperature, which rapidly increases with the onset of solid-solution formation according to Mossbauer spectroscopy experiments.[17,18]

The solid solution phase, although dominated by electron disorder, is far from completely random, implying pockets of local ordering of Li and vacancies.[15,19] The combined lithium ion and electron configurational entropy of the solid solution at the eutectoid transition is only ~0.4 k_b (where k_b is Boltzmann's constant), much lower compared to ~1.39 k_b for a completely random arrangement.[15] The high T behavior of Li_xFePO_4 also provides useful insight about the room temperature solid solution, specifically that there is only a small energetic difference between the phase separated state and the non-equilibrium solid solution. The single-phase state, which has low configurational entropy and becomes thermodynamically stable at relatively low temperature (~400–500 K), must then also have low mixing enthalpy and therefore low room-temperature free energy of Li mixing (assuming the heat capacity does not vary significantly with temperature). First-principles calculations of the room-temperature free energy of mixing confirm this, capping the solid-solution free energy at a maximum of ~15 meV per formula unit (~1.5 kJ per mole, and well below kT at room temperature) above the phase-separated state for the entire Li concentration range.[19] The overall shape of the solid-solution free energy is also quite unusual, as shown in Figure 3a, nearly flat regardless of Li content except approaching zero at the solubility limits (near $x_{Li} \approx 0$ and $x_{Li} \approx 1$), and visualization of the simulated atomic configurations (shown in Figure 3b) reveals considerable short-range ordering of Li and vacancies in the single-phase state. Local ordering of Li and Li-vacancies at room temperature has recently been observed in both partially electrochemically and chemically delithiated $LiFePO_4$ using aberration-corrected annular-bright-field scanning transmission electronic microscopy.[20,21] Also, numerous experimental observations of high T Li_xFePO_4 solid solutions quenched to room temperature remaining stable for extended periods of time,[13,14,22,23] from hours to days, can now be convincingly explained given the characteristic flat mixing free energy which dictates that the thermodynamic driving force for the solid-solution phase to demix is weak.

From probing the bulk phase diagram and performing an analysis of the interactions between relevant species (Li^+, $\square^-$, e^-, h^+) informed by first-principles calculations, the free-energy landscape of Li_xFePO_4 is revealed to be highly nuanced, the implications of which are far-reaching in accurately describing the system's lithiation

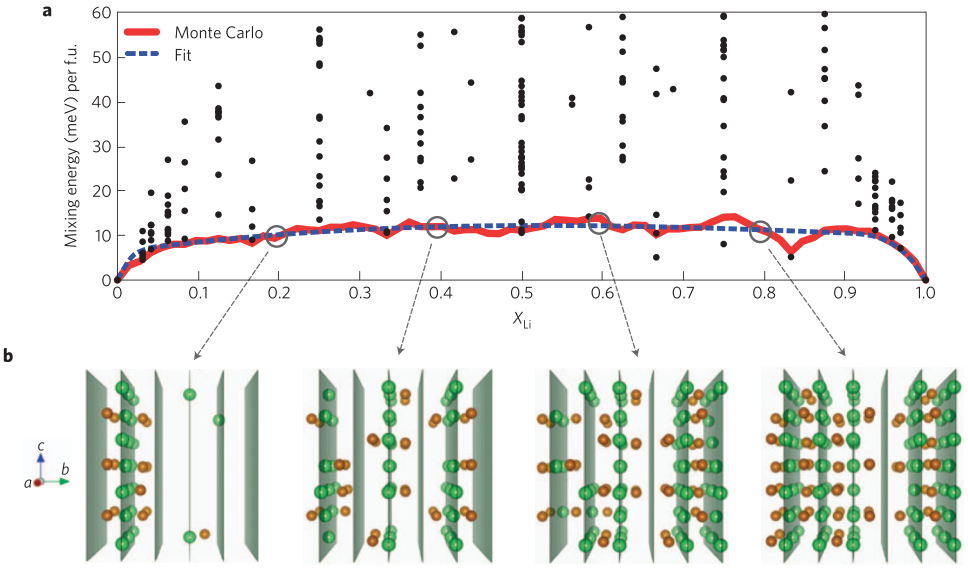

Figure 3. Free energy and atomic configurations along the single-phase $LiFePO_4$ transformation path. (a), Zero-temperature mixing energies (black circles) calculated from first principles of 245 different Li/vacancy and electron/hole configurations in Li_xFePO_4 ($0 \le x \le 1$) show the existence of several low formation energy structures. The non-equilibrium free energy curve at room temperature determined by canonical Monte Carlo simulations (solid red line) using small simulation cells ($2 \times 3 \times 3$ unit cells), as well as the least squares cubic spline fit of the Monte Carlo data (dashed blue) both plateau at ~15 meV per formula unit (f.u.) within $\sim 0.05 < x_{Li} < 0.9$. (b), Snapshots of Li (green atoms) and Fe^{2+} (brown atoms) configurations in Monte Carlo simulations at room temperature for $x_{Li} = 0.2, 0.4, 0.6, 0.8$ show the succession of single-phase states with some local ordering. Adjacent (010) planes containing Li/vacancy are shown in green.[19] Reprinted with permission from Ref. 19, copyright 2011, Nature Publishing Group.

kinetics. Although Li_xFePO_4 is strongly phase-separating at room temperature, the free energy cannot be captured realistically by simplified models (such as a regular solution free energy), which are unfortunately too reductionist insofar as simultaneously capturing local ordering in the solid-solution phase, low free energy of mixing, and correct solubility limits. Because an accurate free energy is a compulsory input parameter for any meaningful modeling of the lithiation kinetics, gross simplification distorts the relative energy of different (de)lithiation pathways, inevitably leading to overall mischaracterization of the charging and discharging kinetics of $LiFePO_4$.

Equilibrium in a single particle

Since $LiFePO_4$ is functionally useful exclusively in nano-form (less than ∼100 nm), the relevant governing thermodynamic potential is no longer the bulk free energy but the single-particle free energy, which now includes significant positive energy contributions from surface and interface (generated as a consequence of intra-particle two-phase coexistence). Overall, these contributions modify the fundamental thermodynamic character of the free energy with resounding implications on charging and discharging.

Van der Ven et al. have specifically investigated how interfacial energy, surface energy, and coherency strains each independently modify the room temperature thermodynamic equilibrium of the $LiFePO_4$ system.[24,25] The change in free energy arises from imposing new physical constraints on the system, of small fixed volume when considering the effects of surface and interfacial energy and fixed lattice parameters (in the directions parallel to the interface) when considering the effect of coherency strain. In general, the imposed physical constraints on a single $LiFePO_4$ particle cause the free energy of the state whereby $LiFePO_4$/$FePO_4$ phase separation occurs within a single particle to vary as a function of the $LiFePO_4$/$FePO_4$ phase fraction. Specifically, the free energy now bows out positively in the two-phase regime, overall inducing some concavity in the free energy as compared to the bulk scenario, illustrated schematically in Figure 4b compared to Figure 4a (note that the solid-solution free energy shown in Figure 3a also shares this feature). This comes as a result of the positive energy penalty (with contribution from both interfacial and coherency strain energy) now introduced to the system to sustain the $LiFePO_4$/$FePO_4$ interface within an individual particle

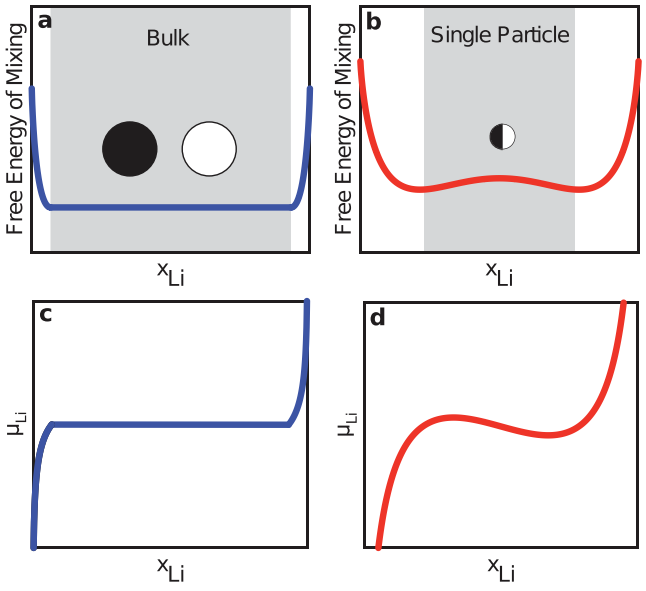

Figure 4. Schematic depictions of (a) the Li_xFePO_4 ($0 \leq x \leq 1$) bulk free energy and (b) the Li_xFePO_4 ($0 \leq x \leq 1$) free energy within a single particle. 2-phase regions are represented in gray. Schematic depictions of the Li chemical potential (μ_{Li}) in (c) bulk Li_xFePO_4 and (d) within a single Li_xFePO_4 particle.

in the two-phase regime (schematically shown in Figure 4b). Because these positive energy contributions only apply in the phase-separated state, the result is the characteristic positive "bump" in the free energy shown in Figure 4b. Not only does explicit consideration of the coherency strain and interfacial energy modify the overall shape of the free energy, but the solubility limits are also affected. The Li concentrations at which the phase-separated state becomes more thermodynamically stable than the single-phase state shift away from the stoichiometric compounds (as seen comparing Figure 4a to Figure 4b) from the bulk to single-particle scenario.[25]

With decreasing particle size, the relative energy penalty per volume associated with interface creation increases, which causes the room-temperature miscibility gap to taper further inward. This trend has also been observed experimentally by Meethong et al. who observe both room-temperature solubility limits to move inward by nearly 0.15 in Li concentration when the particle size is reduced to less than 50 nm,[26] suggesting that below some critical particle size the solid-solution phase may be most stable at all Li concentrations. Similarly, within a single particle the relative interfacial and surface energy penalties per volume vary with the $LiFePO_4$/$FePO_4$ phase fraction depending on the particle morphology, because the interfacial area and the relative surface areas of $LiFePO_4$ and $FePO_4$ may either increase or decrease with phase fraction. Consequently, free energy minimization requires the Li concentration within each of the coexisting phases to change with the phase fraction, meaning that interestingly the solubility limits also vary as a function of overall Li concentration within the particle.[25]

Just the contribution of coherency strain energy to the two-phase free energy is in itself significant: given the approximate 5% difference in volume between $LiFePO_4$ and $FePO_4$ and elastic constants approaching ∼150–200 GPa (the range for c_{11}, c_{22}, c_{33} as determined from first-principles calculations),[27] the two-phase free energy increases by a maximum of nearly ∼1000 J / mol (∼10 meV / formula unit) according to analysis performed by Van der Ven et al. (this for a coherent interface in the *bc* plane, the interface orientation that minimizes the coherency strain energy).[24] Since stresses are relieved at surfaces and elastic strain energy scales with volume, the overall impact of coherency strain compared to interfacial energy increases with crystallite size, in agreement with HRTEM images of partially chemically delithiated large micron-size particles collected by Chen et al. that show the $LiFePO_4$/$FePO_4$ interface aligned along the *bc* plane.[28]

As a consequence of the positive energy penalty incurred from intra-particle two-phase coexistence, not only is the general shape of the free energy uniquely modified as discussed earlier, but the room-temperature metastable solid solution, which already has a remarkably low bulk mixing free energy, becomes relatively more stable in small $LiFePO_4$ particles as the thermodynamic driving force for demixing reduces even further. Experiments by Tan et al. comparing the stability of metastable Li_xFePO_4 solid solutions in nanocrystalline particles to larger particles quenched from high temperature confirm this, showing that nano-Li_xFePO_4 solid solutions not only persist for longer before decomposing but also are stable at lower annealing temperatures.[29] This is a somewhat surprising finding, given that with decreasing particle size the ratio of possible surface nucleation sites to bulk sites increases, which should favor heterogeneous nucleation.

In both cases, of either phase-separation within a single particle, or metastable solid solution, the free energy qualitatively resembles that portrayed in Figure 4b with some inherent and irremovable non-convexity, as opposed to the bulk scenario shown Figure 4a. Moreover, there is *no* scenario where the Li_xFePO_4 free energy within an individual particle is entirely flat or convex. Therefore, the single-particle Li chemical potential, defined as the instantaneous slope of the free energy with respect to Li concentration, resembles the curve shown in Figure 4d as opposed to Figure 4c. The single-particle voltage curve (related through $\Delta\phi = -\Delta\mu_{Li}$ and discussed in detail in the Appendices section, where ϕ is the cell potential and μ_{Li} is the Li chemical potential), however, strongly differs from the experimental open-circuit voltage curve, which exhibits the characteristic

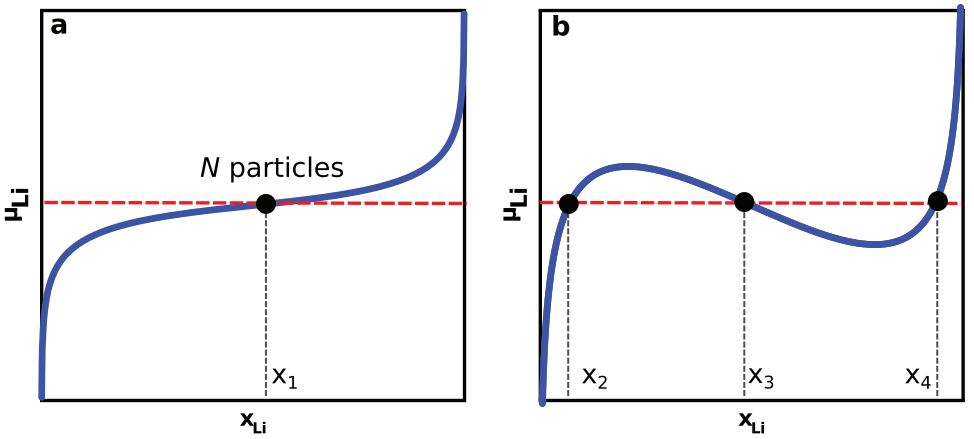

Figure 5. Schematic depictions of the equilibria defined at some fixed μ_{Li} (dashed red line) in a multi-particle system of N particles, each with either **(a)** a monotonically increasing single-particle Li chemical potential (μ_{Li}) or **(b)** a non-monotonically increasing single-particle Li chemical potential (μ_{Li}).

plateau for almost the entirety of the Li concentration range (like that shown in Figure 1). This can only be reconciled by studying how the thermodynamic equilibrium is again redefined in an ionically and electronically interconnected network of $LiFePO_4$ particles.

Multi-particle equilibrium.— An actual composite electrode is an assembly of many particles ($\sim 10^{10}$–10^{17}), no longer subject to the constraint that the Li concentration must remain fixed within each particle only that the overall Li concentration in the electrode is set. For an electrochemical cell to function, the active cathode material must be ionically and electronically wired to the counter-electrode, and in the conventional Li-ion battery architecture, active particles are simultaneously ionically and electronically wired to each other (through the electrolyte facilitating Li^+ exchange and through either carbon addition and/or particle–particle contact ensuring electronic connectivity). Li exchange between $LiFePO_4$ particles has been shown experimentally by Lee et al.,[30] by first constructing an electrode consisting of nano-$FePO_4$ and bulk $LiFePO_4$ particles and, after allowing the system to equilibrate, observing peak broadening in the X-ray diffraction (XRD) spectra consistent with the existence of nano-$LiFePO_4$. It is typically assumed that measurements of multi-particle systems reflect single-particle behavior, which may be a reasonable assumption for solid-solution systems but, as we show below, falls short in describing phase-separating systems.

The multiple particle equilibrium differs from the single-particle equilibrium due to the characteristic non-convexity of the single-particle free energy. The conditions for equilibrium in a multiple particle assembly (i.e. to minimize the system free energy) require all particles to have identical μ_{Li} and to be stable with respect to Li concentration exchange fluctuations between particles. If the single-particle free energy is entirely convex, the corresponding μ_{Li} monotonically increases with x_{Li} as shown in Figure 5a, and thus for a given μ_{Li} there is a unique global minimum in the system free energy corresponding to all N particles sharing the identical Li concentration (x_1). Due to the non-convexity in the single-particle free energy (highlighted in Figure 4b), however, the $LiFePO_4$ single-particle μ_{Li} does not increase monotonically with x_{Li}, and there are several different x_{Li} (namely x_2, x_3, and x_4) that share the same μ_{Li} (shown in Figure 5b), meaning that there are multiple configurations that satisfy the first equilibrium criterion (identical μ_{Li} in each particle). Dreyer et al. have enumerated through all possible equilibria, showing that for a given global Li concentration, there are stable equilibria each corresponding to a fraction of the particles Li-rich and the remaining fraction Li-poor.[31] Physically, this can be rationalized by considering that the possibility of free Li-exchange amongst all particles allows any energy penalty associated with creating a two-phase interface in a single particle to be avoided. Coexistence of fully intercalated and deintercalated $LiFePO_4$ particles has indeed been confirmed in partially electrochemically lithiated samples allowed to relax and then characterized using both ex-situ X-ray diffraction (XRD)[32] and advanced transmission electron microscopy (TEM) methods.[33] It is of interest to point out that the aforementioned ex-situ observations of fully lithiated and delithiated particles can be fully rationalized by the system thermodynamics without having to invoke any specific kinetic mechanism of lithiation.

The consequences of having multiple local minima in the free energy can be illustrated with a demonstrative example. Consider the simplified case illustrated in Figure 6, a system containing 4 identical Li_xFePO_4 particles with a global concentration falling within the single-particle miscibility gap ($x_{Li} = 0.4$). Highlighted and overlaid over the schematic single-particle free energy in Figure 6 are two configurations corresponding to two local minima, one consisting of 2 lithium poor and 2 lithium rich particles (labeled [2,2] in red) and another consisting of 3 lithium poor and 1 lithium rich particles (labeled [3,1] in green). The molar free energy of the system is graphically represented at $x_{Li} = 0.4$ by the red and green points, the molar free energies of the [2,2] and [3,1] configurations, respectively. Although there is only a small difference in the free energy between both equilibria, there is a notable difference in μ_{Li} (and consequently the open-circuit voltage), represented by the slope of the tangent of the free energy, drawn in red and green for the [2,2] and [3,1] configurations, respectively. In Li_xFePO_4, the open-circuit voltage of different equilibria can vary by as much as ~20 to 30 mV, while maintaining near identical free energy (~5–10 meV/f.u. or 1–2 kJ/mol) according to Figure 3a. As more particles are introduced to the system, the num-

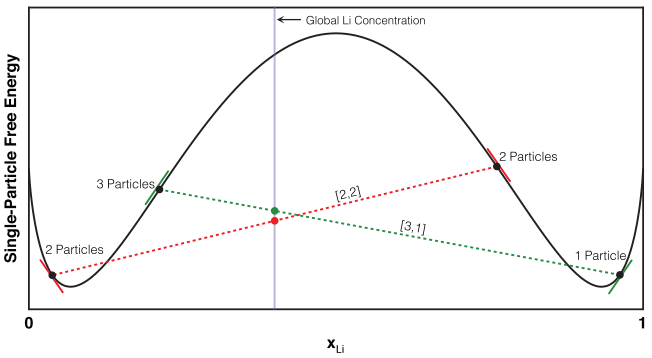

Figure 6. Illustration of the existence of two possible local equilibria (labeled [2,2] in green and [3,1] in red) in a 4-particle system with global concentration $x_{Li} = 0.4$, where each particle has an identical non-convex single-particle free energy (drawn in black). The Li chemical potential (μ_{Li}) of each equilibrium is represented by the instantaneous slope of the single-particle free energy (i.e. slope of solid green or red tangent).

ber of such equilibria also increases, and by virtue of having many stable equilibrium configurations, the equilibrium that a system eventually evolves toward is *path-dependent*, which is reflected in OCV measurements with varying charging and discharging histories converging to different values (even after long relaxation times).[31,34,35] This feature of the free energy landscape of $LiFePO_4$ effectively rationalizes how the Li_xFePO_4 system well known for rapid lithiation kinetics appears to require exorbitant times to equilibrate as entire particles must transform as the system evolves toward a local free-energy minimum.[31] Even though the voltage change between these different local equilibria is small, the overall state of the electrode is very different.

In a potential-controlled system like an electrochemical cell, the existence of a non-monotonic single-particle voltage curve and interaction between active particles are chiefly responsible for the characteristic voltage plateau observed in slow discharging and charging experiments.[31] The subset of equilibria traversed during low-rate charging is shown qualitatively in Figure 7. To charge an assembly of $LiFePO_4$ particles quasi-statically, a small overpotential (the difference between Φ_{app} and the single-particle potential in Figure 7) is continually applied to drive Li out of $LiFePO_4$. Initially the driving force for charging, which is the difference between the applied potential and the single-particle potential, *decreases* with respect to further Li removal from a single particle, simply because the single-particle potential initially increases with capacity. Thus for charging several particles, this ensures that Li is extracted equally from all particles within this regime, as shown schematically in Figure 7a and Figure 7b.

Once the potential is increased such that each particle reaches the critical concentration x_c (Figure 7c), there is an apparent concentration instability– any fluctuation of Li out of an individual particle begets additional accelerated Li removal, as the driving force for charging increases in the already delithiating particle (described schematically with arrows of increasing magnitude in Figure 7c delineating the accelerated charge of Particle 1). Whether the Li is removed to the counter-electrode or is incorporated into neighboring particles (i.e. Particles 2,3, or 4) will depend on the electrode kinetics. At this same potential, the process repeats itself and the remaining lithiated particles charge sequentially, as described in Figure 7e and Figure 7f, which accounts for the well-observed voltage plateau in experiments shown schematically in Figure 7g. Due to the shape of the single-particle voltage curve, the voltage plateau for the multi-particle system is inherently higher on charge than on discharge, which explains the non-vanishing ~20 mV hysteresis in the zero-current limit (at C/1000) in the Li_xFePO_4 voltage profile demonstrated by Dreyer et al.[31]

The particle size and morphology distribution of the active particles within the electrode means there is also a distribution amongst the active particles' phase transition voltages due to variation in the surface energy contributions to each single-particle free energy. Van der Ven et al. studied the effect of particle size distribution on the multi-particle Li_xFePO_4 OCV and showed that the larger the surface energy difference between a lithiated and delithiated active particle, and the wider the particle size distribution (within the nano-particle regime where surface-energy effects contribute the greatest), the more sloping the open-circuit voltage curve becomes.[36]

Across length scales, from bulk, to single-particle, to an assembly of many particles, the additional interactions and physical changes to the system continually modify the Li_xFePO_4 free energy and voltage profile. *Therefore, the free energy and voltage of a multiple-particle $LiFePO_4$ system appears qualitatively differently than that of a single particle, which in itself has varying features compared to the bulk system.* Since the vast majority of electroanalytical experiments are performed on electrodes consisting of many particles, the behavior of single-particle Li_xFePO_4 is shrouded by interactions between particles, which can lead to possible mischaracterization of the properties of individual $LiFePO_4$ particles, an oft-recurring theme in the $LiFePO_4$ literature. For instance, the appearance of a voltage plateau in slow galvanostatic charging and discharging experiments has been historically interpreted as all $LiFePO_4$ particles simultaneously undergoing a phase transformation with two-phase coexistence, but as revealed through analysis of the multi-particle equilibrium, the plateau in the open circuit voltage really signifies coexistence of nearly fully lithiated and delithiated active particles, and no statement about *how* particles individually transform can be made from these experiments. Alternatively, sloping voltage curves are conventionally interpreted as proof of single-phase existence and are often used in the literature to identify the solubility limits; however, as demonstrated by Van der Ven et al., a sloping voltage curve can arise from a wide size distribution of nano-particles each undergoing a phase transformation. Overall, a thorough examination of the Li_xFePO_4 equilibrium at the relevant length scales (bulk, single-particle, multi-particle) reveals the apparent non-triviality of the system thermodynamics

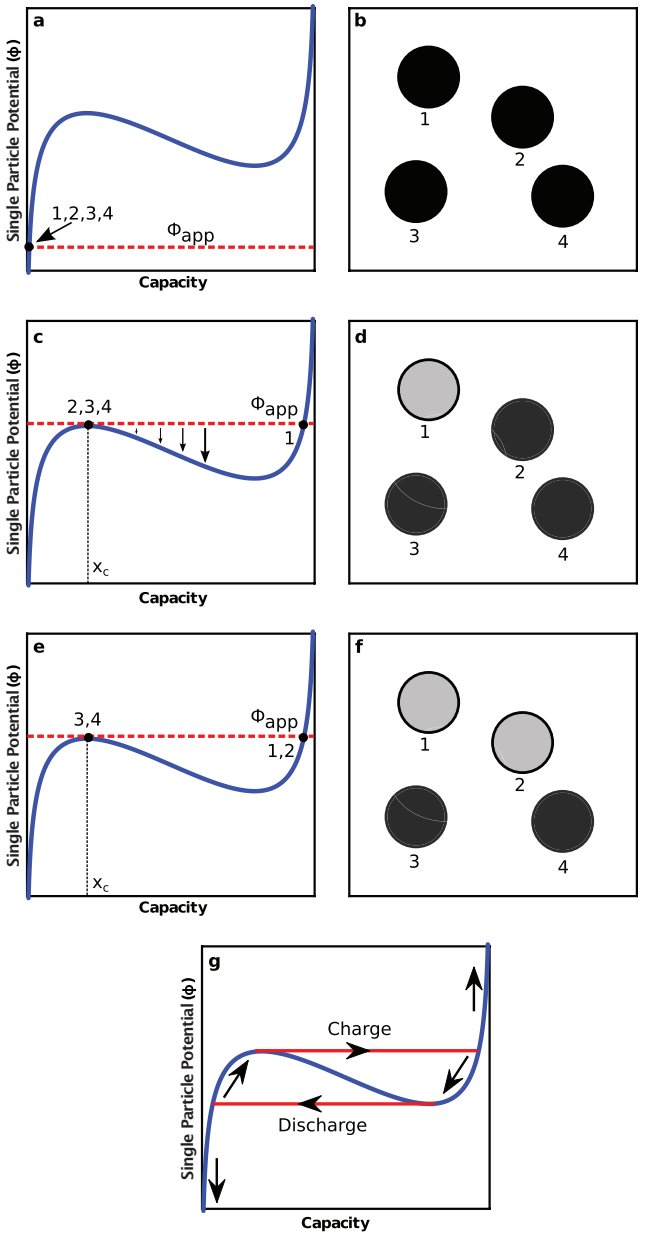

Figure 7. Schematic illustration of slow (quasi-static) charging, with some slowly increasing applied potential Φ_{app} (dashed red line), of a 4-particle Li_xFePO_4 system where each particle has the single-particle potential (drawn in blue) described in (a), (c), and (e). Qualitative descriptions of each particle's concentration during the charging process are described schematically (b), (d), and (f). The total system behavior is highlighted in (g) which shows the system voltage curve with characteristic built-in hysteresis in the zero-current limit.

providing the basis for the unique (de)lithiation kinetics observed in this material. One may have to accept that simple charge/discharge experiments on composite electrodes reveal very little about the delithiation curve of single particles.

$LiFePO_4$ Kinetics – Bulk, Single-Particle, Multi-Particle

Bulk Kinetics

Li diffusivity in $LiFePO_4$.— In a material first mischaracterized as low-rate, and later revealed to be high-rate, the bulk Li diffusivity in $LiFePO_4$ has been one of the many issues of contention in the research literature over the past several years. From a variety of both computational and experimental techniques, the room temperature Li diffusivity has been reported to be as low as $\sim 10^{-16}$ cm^2/s and as high as $\sim 10^{-8}$ cm^2/s, clearly an unacceptable discrepancy for such a closely studied material. The type of method used to characterize the diffusivity has a great effect in influencing the measured value precisely because of the interplay of effects at the bulk, single-particle, and multi-particle scales. For example, a conventional electroanalytical method to determine the diffusion coefficient involves performing cyclic voltammetry, assuming Cottrell-like behavior, and observing the trend in the peak current as a function of potential scanning rate.[37,38] Another common method involves using the galvanostatic intermittent titration technique (GITT), where the chemical diffusion coefficient is ascertained from the voltage response to applied current pulses.[39,40] Electro-impedance spectroscopy (EIS) methods have been used to deduce the diffusivity typically by invoking the Randles equivalent circuit, and extrapolating the Warburg impedance from a Nyquist plot.[37,39,41–43]

From all three methods (CV, GITT, EIS), the extracted diffusivity cannot reflect the Li diffusivity in $LiFePO_4$ because of a critical but unreliable assumption made in all of these techniques: all particles *do not* simultaneously participate when the entire electrode is charging or discharging. In fact, in the slow charging/discharging limit, the majority of particles remain idle at any given snapshot in time. The lithiation/delithiation behavior at the single-particle scale, therefore, is not mirrored at the multi-particle (electrode) scale. This general mischaracterization manifests itself from either the assumption of solid-solution behavior, and thus linear diffusion, in all particles (which implies a much more homogeneous lithiation scheme) or identical 2-phase behavior in all particles. As rigorously elucidated by Dreyer et al.,[31] $LiFePO_4$ particles transform sequentially in the zero current limit, implying that in employing the conventional electroanalytic methods discussed here, only a subset of particles are active in taking up or expelling Li. As most papers assume that all the active mass participates, the gross overestimation of the active surface area results in artificially low calculated and reported Li diffusivities. This general phenomenon has been sparsely recognized in the literature, and the diffusivities calculated from these methods are often relabeled as 'apparent' or 'effective' diffusivities which strongly depend on the electrode architecture and thus do not reflect the actual Li conductivity in bulk $LiFePO_4$.[38,39] For example, Liu et al.[42] use conventional CV and EIS methods to conclude that the effective Li diffusivity improves as more carbon black is added at the electrode level, implying that the overall electrode kinetics may be improved, but certainly the calculated diffusivity does not reflect that of bulk $LiFePO_4$, which should remain unchanged regardless of carbon black content. To this end, Gaberscek et al.[44–46] share similar misgivings and question conventional EIS interpretation, systematically illustrating the significant contributions from electrode architecture (external pressure applied to the electrode, electrochemical 'wiring', etc.) on collected impedance spectra, and have accordingly sought to develop more precise and involved equivalent circuits capable of decoupling single-particle from-multi particle kinetics. The real issue is, however, that electrode architecture controls the amount of mass that is active in a given potential or current step, and it is uncharacterized "participation rate" that makes diffusion constants extracted from composite electrodes meaningless.

The challenges encountered in trying to determine accurately the bulk Li diffusivity in $LiFePO_4$ from classical electroanalytical methods call for more localized measurement techniques which remain unconvoluted by multi-particle interactions. In this regard, atomistic computational models are particularly adept at describing local Li migration.[47,48] Morgan et al. first calculated the intrinsic Li ion diffusivity in $LiFePO_4$ from first-principles methods and found that room temperature Li conduction is especially rapid ($D_{Li} \sim 10^{-8}$ cm^2/s) along 1D tunnels oriented in the [010] direction illustrated in Figure 8 and negligible along perpendicular directions ([001] and [101]).[47] Islam et al. confirmed this finding, identifying the same anisotropic local Li migration behavior using empirical potentials.[48] Also, unpublished ab initio molecular dynamics simulations performed by our research group yield comparable diffusivities to those obtained by Morgan et al. ($\sim 10^{-7}$–10^{-9} cm^2/s) along the [010] direction. All of these computational findings were further validated when Nishimura et al. confirmed experimentally the same favored direction of Li motion by visualizing the positions of Li atoms in neutron diffraction experiments.[49] The local migration behavior of Li in $LiFePO_4$ was recently examined quantitatively by Sugiyama et al.[50] who measured muon-spin rotation and relaxation spectra in polycrystalline $LiFePO_4$ samples and estimated D_{Li} to be $\sim 3.6 \times 10^{-10}$ cm^2/s at room temperature, much nearer to the values determined from first-principles calculations than to experiments. The verification of rapid Li diffusivity in $LiFePO_4$ is especially reassuring in that it resolves the apparent mystery of how a cathode material can perform exceptionally well at rapid rates despite having supposedly poor bulk transport properties, as (incorrectly) obtained from electrode experiments.

Measurements of local Li migration may be accurate in describing transport in pristine bulk $LiFePO_4$ unmarred by defects, but Li transport is modified[51–53] and becomes particle size dependent[52] in realistic, defective material. The most common point defect, the nearest neighbor Li–Fe antisite, involves Fe^{2+} residing directly in the fast 1D diffusion path as described and shown in the Appendices, which impedes rapid Li migration along the *b* axis. A discussion of the types

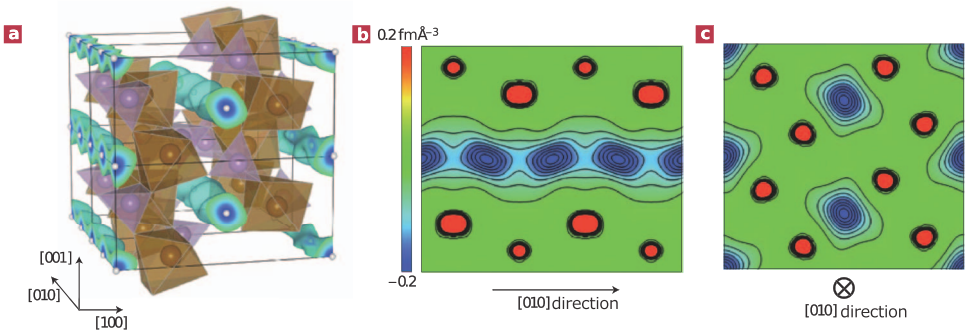

Figure 8. Fast 1D diffusion paths oriented along the [010] direction as observed by measuring the Li nuclear density (blue contours) by Nishimura et al.[49] Reprinted with permission from Ref. 49, copyright 2008, Nature Publishing Group.

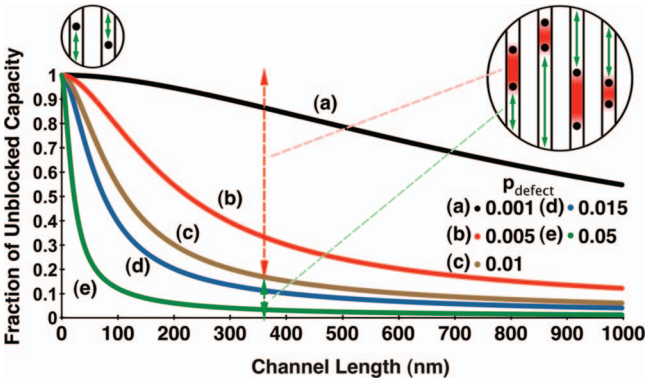

Figure 9. Variation with defect concentration of expected unblocked capacity (defined as the capacity situated between the two furthest anti-site defects residing within the same [010] channel, shown schematically in red) vs channel length in $LiFePO_4$ particles, assuming defect creation is a Poisson process and defects are spatially uniformly distributed, as determined by Malik et al.[52] Reprinted from Ref. 52, copyright 2010, The American Chemical Society.

and formation energies of point defects in $LiFePO_4$ is presented in the Appendices. As soon as there are two such defects within the same 1D diffusion channel, the capacity situated in between cannot be accessed without circumventing at least one such defect obstruction, as illustrated in Figure 9. The particle size effect here is apparent–given a constant defect concentration, the larger the particle size, the greater the fraction of capacity that is 'blocked,' assuming a uniform spatial distribution of defects.[52] The effective ionic diffusivity in a particle now depends on two factors, the concentration of obstructing defects and the particle size. Taking these factors into account, Malik et al.[52] have recalculated the directional diffusivities (along the *a*, *b*, and *c* directions), showing that at room temperature the diffusivity along the [010] decreases by over two orders of magnitude (from $\sim 10^{-8}$ cm^2/s to $< \sim 10^{-10}$ cm^2/s) with the introduction of just 1% defect concentration. The overall anisotropy of Li diffusion decreases as the presence of antisite defects simultaneously facilitates easier migration along the [101] direction enabling 'cross-over' to adjacent channels, effectively changing the Li migration mechanism from one dimension to two or three.[52,53] These general findings are supported in single-crystal conductivity measurements[54–56] (performed in mm-size crystals, which consequently have near 100% blocked capacity, using blocking electrodes) that display the expected drop in the Li diffusivity along the *b* axis and similar diffusion anisotropy compared to that predicted for defective $LiFePO_4$. Also, the increased obstruction of fast 1D Li diffusion in larger particles caused by the presence of immobile point defects in the migration path effectively rationalizes the enhanced rate performance observed in nano-$LiFePO_4$ compared to micron-size $LiFePO_4$, a scaling improvement that exceeds that predicted from Fick's Laws. However, even with diffusivity $\sim 10^{-10}$ cm^2/s for defective $LiFePO_4$ particles, Li diffusion is still very fast, and much faster than what is deduced from multi-particle electrode measurements.

The overall complexity of Li ion conduction in $LiFePO_4$ becomes immediately apparent from an exhaustive survey through the literature, where several seemingly contradictory values of the Li diffusivity have been reported, leading some to conclude that $LiFePO_4$ is a poor ionic conductor and others the opposite. By thoroughly understanding how the apparent diffusion behavior is modified from bulk, to a single particle, to many particles, the gulf in measured diffusivities is readily explained: local Li diffusion in $LiFePO_4$ is especially rapid along the [010] channels (likely $\sim 10^{-8}$ to 10^{-9} cm^2/s at room temperature) and negligible along perpendicular directions, but in the presence of obstructing point defects the diffusion anisotropy and overall diffusivity along the [010] direction are drastically reduced, and in electrode-scale measurements calculated Li diffusivities are artificially low by virtue of only a fraction of the active particles participating in Li uptake or expulsion (at low rate) and hence are not appropriate.

Electronic conductivity.—Like the Li diffusivity, there have been many studies focused on characterizing electronic conductivity of $LiFePO_4$, again with reported values spanning several orders of magnitude. Much of the literature reports the bulk electronic conductivity as simply 'poor' (10^{-7}–10^{-9} S/cm[55,57] for the lithiated phase and $\sim 10^{-11}$ S/cm for the delithiated phase[58]), but its role in the charging and discharging process, specifically whether or not it is rate-limiting, remains unclear. The challenges in measuring bulk electronic conductivity and interpreting electronic conductivity measurements are multiple and will be explored in this section.

The mechanism responsible for electronic transport in bulk $LiFePO_4$ is, however, well understood and is not a source of contention in the literature. Electronic conduction in the mixed valence state proceeds through thermally activated small polaron hopping. As discussed earlier, the electron associated with the Fe^{2+}/Fe^{3+} redox localizes on the transition metal sublattice. A small polaron is defined as the 'quasiparticle' comprised of the localized electron (or hole) and its induced polarization field that distorts the local crystal. In the migration process both the electron (or hole) and its associated local distortion move together[59] on a 2D plane defined by the transition metal sublattice (*bc* plane). The electronic conductivity, therefore, is determined largely by two parameters, namely the activation energy for electron migration and the concentration of charge carriers (which is set extrinsically by impurities or by the Li concentration). This dependence is expressed in equation 1:

$$\sigma \propto n \exp\left(-\frac{Em}{kT}\right) \quad [1]$$

where σ denotes the conductivity, T the temperature, n the carrier concentration and E_m the polaron migration barrier.

Two common electrochemical methods used to characterize the electronic conductivity are electrical impedance spectroscopy (EIS) and the four-point Van der Pauw DC method. EIS involves first measuring the current response at different frequencies and then using equivalent circuit models to infer the electronic conductivity, while the four point Van der Pauw method determines the resistivity of a thin sample by measuring the voltage response to an applied DC current. Each of these techniques employs ionically blocking electrodes, making electrons the only contributors to the observed current. Electronic conductivities obtained from electrochemical measurements are generally in the 10^{-7}–10^{-9} S/cm range,[55,57] which is significantly lower than the conductivity of other cathode materials such as Li_xCoO_2 ($\sim 10^{-1}$ S/cm for a single crystal in the semiconductive $x = 1$ phase).[60] This has led many in the battery community to label electron transport as the rate-limiting process in $LiFePO_4$.

There are, however, important challenges regarding the interpretation of measurements derived from classical electrochemical methods. The difficulty in decoupling conductivity in the active material from electrode-scale resistance and the physical relevance of decoupling ionic and electronic motion call into question the common belief that electron transport is rate limiting in $LiFePO_4$. The first important challenge associated with the use of classical electrochemical methods lies in the interpretation of multi-particle measurements, in which electronic conductivity within particles must be separated from electronic resistance at the electrode scale. Sources of electrode-scale resistance include contact resistance between the current collector and the composite electrode, contact resistance between the active materials and the carbon conductive network and contact resistance at the boundary between particles.[57] For example, Delacourt et al.[57] reported a 7 order of magnitude increase in electronic conductivity going from pure $LiFePO_4$ (10^{-9} S/cm) to carbon-coated $LiFePO_4$ (10^{-2} S/cm). As stated by the authors, such an increase in conductivity cannot be attributed to the particles themselves, but can be understood rather as a signature of the percolating conducting network formed by the carbon coating. This analysis suggests that the method employed, in this case

EIS, was unable to capture strictly the electronic conductivity within single particles.

The multi-scale nature of electronic conductivity in composite electrodes is readily seen with broadband dielectric spectroscopy (BDS) which, using frequencies ranging from 40 to 10^{10} Hz (an extended frequency range compared to standard EIS), can identify charge fluctuations at different length scales in the electrode. As the frequency of an electromagnetic wave increases, its wavelength decreases, making high frequency waves ideal for probing the dynamics of electron transport at small length scales. Conversely, low frequency waves can be used to assess electronic transport at larger length scales. Using BDS, Seid et al.[61] identified conductivities ranging from 10^{-6} S/cm to 10^{1} S/cm, respectively indicative of electrode-scale conduction and carbon coating conduction. This study, however, was also unable to isolate the electronic conductivity within $LiFePO_4$ particles themselves. This may be an indication that at the length scale at which electronic transport within single particles occur the recorded current response is dominated by other forms of electronic transport, such as electronic transport within the carbon coating network.

Several strategies have been employed in the literature in order to isolate particle conductivity from electrode scale conductivity. One approach employed by Amin et al.[54,55] involves performing measurements on large mm-size single crystals. AC impedance spectroscopy as well as DC polarization/depolarization measurements were performed on large millimeter-sized $LiFePO_4$ crystals, leading to a 2D electronic conductivity in the *bc* plane on the order of 10^{-7} S/cm at 50 °C.[55] Similar measurements with electronically blocking electrodes found the ionic conductivity to be approximately 4 orders of magnitude less than the electronic conductivity at high temperature (140°C), thus identifying ionic transport as opposed to electronic transport as the rate-limiting process in Li transport. This conclusion challenges the common belief that electronic conductivity is rate-limiting in $LiFePO_4$. However, although valid for large millimeter-sized particles, this conclusion cannot be generalized necessarily to nano-sized particles, due to the particle size dependence of the ionic conductivity arising from channel-blocking point defects (as discussed in the *Li Diffusivity in $LiFePO_4$* section).

Another experimental approach to isolate particle-scale from electrode-scale conductivity consists of directly measuring the polaron hopping rate between adjacent Fe atoms using Mossbauer spectroscopy. Mossbauer spectroscopy is able to detect local changes in the oxidation states of iron atoms with high spatial and temporal resolution using isomer shifts in the gamma ray absorption spectrum of Fe nuclei. Using this method, Tan et al.[62] found polaron migration barriers ranging between 0.3 and 0.41 eV for fully delithiated and fully lithiated particles, respectively. These values are on the low end of the experimentally measured polaronic activation barriers, which are mostly reported to be in the 0.4–0.6 eV[57,63] range. Notable exceptions are the low activation barriers reported by Takahashi et al. (0.155 eV, using EIS)[37] and Shi et al. (0.189 eV using DC measurement on a pressurized sample).[63]

Polaronic activation barriers can also be assessed by theoretical methods based on first principles. Using DFT, Maxisch et al.[59] reported activation barriers ranging from to 0.175 eV to 0.215 eV in the fully delithiated and fully lithiated limits, respectively. These barriers are comparable to previously calculated lithium-ion migration barriers (0.2–0.27 eV), once again challenging the belief that electronic mobility is the rate-limiting step in $LiFePO_4$. The method, however, does not take into account the binding energy between a polaron and its nearest lithium ion. This binding energy was calculated by Maxisch et al. to be on the order of 0.5 eV, indicating that ionic and electronic migration in $LiFePO_4$ is likely coupled. This finding leads to the second important challenge in interpreting electronic conductivity measurements, namely the physical relevance of separately measuring ionic and electronic conductivities to assess rate capabilities. During electrochemical (dis)charging, Li^+ and e^- simultaneously diffuse within a particle and, as determined from first-principles calculations, this motion is likely to be coupled. This claim is supported by the aforementioned high Li^+/polaron binding energy (Maxisch et al.) as well as by a recent DFT investigation by Sun et al.[64] which finds a strong correlation between Li^+ and e^- migration paths during Li transport.

Ambipolar lithium diffusivity, which captures the aggregate effect of Li^+ and e^- migration, emerges as a more relevant quantity to describe electrochemical processes. Several experimental methods described in the *Li Diffusivity in $LiFePO_4$* section, such as cyclic Voltammetry, PITT, and GITT, involve partial (de)lithiation of $LiFePO_4$ particles and therefore attempt to capture the coupled motion of Li^+ and e^- during electrochemical (dis)charging processes. However, methods that separately measure ionic or electronic conductivities at fixed lithium concentration, such as EIS or Four Point Van der Pauw, by definition cannot capture such coupled motion. Analysis of data provided in the literature shows that ambipolar diffusivity cannot simply be extracted from the separate investigation of electronic and ionic conductivities. Ambipolar diffusivity can indeed vary significantly from the prediction of mean-field models, which relate ambipolar diffusivity to electronic and ionic diffusivity in the case of non-interacting charged species. The predictions of ambipolar diffusivity from mean field models is a two-step process that is expressed in equations 2 and 3. Equation 2, known as the Nernst-Einstein equation, is used to relate ionic conductivities to ionic diffusivities. The mean-field approximation is expressed in equation 3, which relates the ionic diffusivities to the ambipolar diffusivity in the case of an ideal solution of non-interacting charged species.

$$D_i = \frac{\sigma_i kT}{c_i q^2} \quad [2]$$

$$\tilde{D} = \frac{2D_{Li+}D_{e-}}{D_{Li+} + D_{e-}} \quad [3]$$

In equations 2 and 3, σ_i is the conductivity of species i, c_i is the carrier concentration of species i, D_i is the diffusivity of species i and $\tilde{D}$ is the ambipolar diffusivity.

An example of the discrepancies between the predictions of mean field models and the measured ambipolar diffusivities can be seen from the work of Amin et al.[55] At 450 K, Amin et al. measured the electronic and ionic conductivities using EIS to be 10^{-4} S/cm and 10^{-8} S/cm, respectively, and the ambipolar diffusivity was found using DC polarization measurements to be on the order 10^{-8}–10^{-9} cm^2/s. The mean-field model approach expressed in equations 2 and 3 would predict the same ambipolar diffusivity to be $\sim 10^{-19}$ cm^2/s, which is eleven orders of magnitude smaller than the measured value (a 5% carrier concentration was assumed in this calculation, as determined from the solubility limits of $LiFePO_4$ at 450 K[14]). This highlights the fact that the coupled motion of Li^+ and e^- is not simply the sum of two independent ionic motions, and therefore questions the use of ionic and electronic conductivities as a metric for rate capabilities.

Nevertheless, the idea that electronic conductivity is rate-limiting in $LiFePO_4$ is still widely accepted in the literature. To address the purported electronic conductivity issue, there have been several studies of doping $LiFePO_4$ in an attempt to improve the bulk electronic conductivity. And, to this end, reported conductivities of doped $LiFePO_4$ have been as high as 10^{-1} S/cm and excellent rate performance has been obtained in cycling experiments with doped $LiFePO_4$.[5] Whether these improvements arise from improving the bulk electronic conductivity or not remains an unresolved issue of contention in the literature and is beyond the scope of this work.

In summary, although it is generally believed to be low, no consensus has been reached on the true value of the bulk electronic conductivity in $LiFePO_4$, and the jury is still out on whether or not electron migration is the rate-limiting step in this material. Nevertheless, in electrochemical systems the independent ionic and electronic conductivities as measured from the current response to an electric field at a fixed lithium concentration may not be a direct predictor of rate performance. The coupled $Li^+ - e^-$ migration during electrochemical processes where Li^+ and e^- are supplied externally determines the true rate at which the electrochemical reaction can proceed, which for nano-sized $LiFePO_4$ has proven to be very high.

Single-particle lithiation mechanism

Given the strong phase-separating behavior of Li at room temperature, the extremely high rate performance of $LiFePO_4$ is certainly puzzling upon first inspection. As initially noted by Padhi et al., Li insertion and removal through propagating a two-phase $LiFePO_4/FePO_4$ interface within an active particle can only hinder the overall discharging and charging kinetics (in comparison to a solid-solution mechanism), which motivated the initial conclusion that $LiFePO_4$ would be best suited for low-rate applications.[1] Therefore, elucidating the single-particle lithiation mechanism is critical not only to explain why $LiFePO_4$ can function as a high-rate material, but also to clarify the requisite criteria for identifying new high-rate two-phase battery electrode materials that can behave similarly.

Unfortunately, uncovering the single-particle lithiation mechanism poses significant challenges. First, because most conventional electroanalytic characterization methods are performed on bulk electrodes containing many particles, the single-particle lithiation mechanism is obfuscated in the extracted data by the multi-particle behavior and ensuing electrode-scale inhomogeneity. Second, because lithiation is a dynamic process, direct characterization then requires in-situ single-particle experiments, which require both temporal and spatial precision beyond the limits of current experimental characterization methods. Consequently, the majority of experiments investigating the $LiFePO_4$ lithiation mechanism fall into two broad categories with their respective built-in tradeoffs: either ex-situ analysis on relaxed single particles, or conventional electroanalytic characterization of charging or discharging bulk electrodes (i.e. galvanostatic voltage curves, PITT, GITT, CV, etc.). Nevertheless, these limitations have not prevented ample progress in recent years toward understanding the $LiFePO_4$ single-particle lithiation mechanism, as carefully designed experiments and models have now shed light on why $LiFePO_4$ is capable of being rapidly charged and discharged.

Isotropic two–phase models.— Inferred from the characteristic flat $LiFePO_4$ voltage curve, the most intuitive lithiation models all involve intra-particle two-phase coexistence, where on discharge the $LiFePO_4$ phase grows at the expense of $FePO_4$ and the reverse occurs upon charge. Padhi et al. first described a "core-shell" process as shown schematically in Figure 10a and Figure 10c, and in the years following this general model has been refined and modified to take into account the Li diffusion anisotropy, coherent strain energy, dimensionality of the rate-limiting growth mechanism, etc., with some notable examples depicted in Figure 11. In the "core-shell" scheme, the reaction front upon both Li insertion and extraction moves radially inward, meaning that the interfacial area shrinks with time. This feature of the model was initially used to explain how at higher currents, the shrinking interfacial area becomes a current bottleneck and consequently limits the accessible capacity.[1] Similarly, the "mosaic model" proposed by Andersson et al. accounts for inaccessible capacity as the result of growing $FePO_4$ domains (on charge, for instance) impinging upon each other leaving unconverted $LiFePO_4$ in between (shown in Figure 10b).[65] Through carbon addition and reducing the particle size (to ∼100 to 150 nm), however, close to the entirety of the theoretical capacity (∼170 mAh/g) becomes accessible even at high rates,[3] which

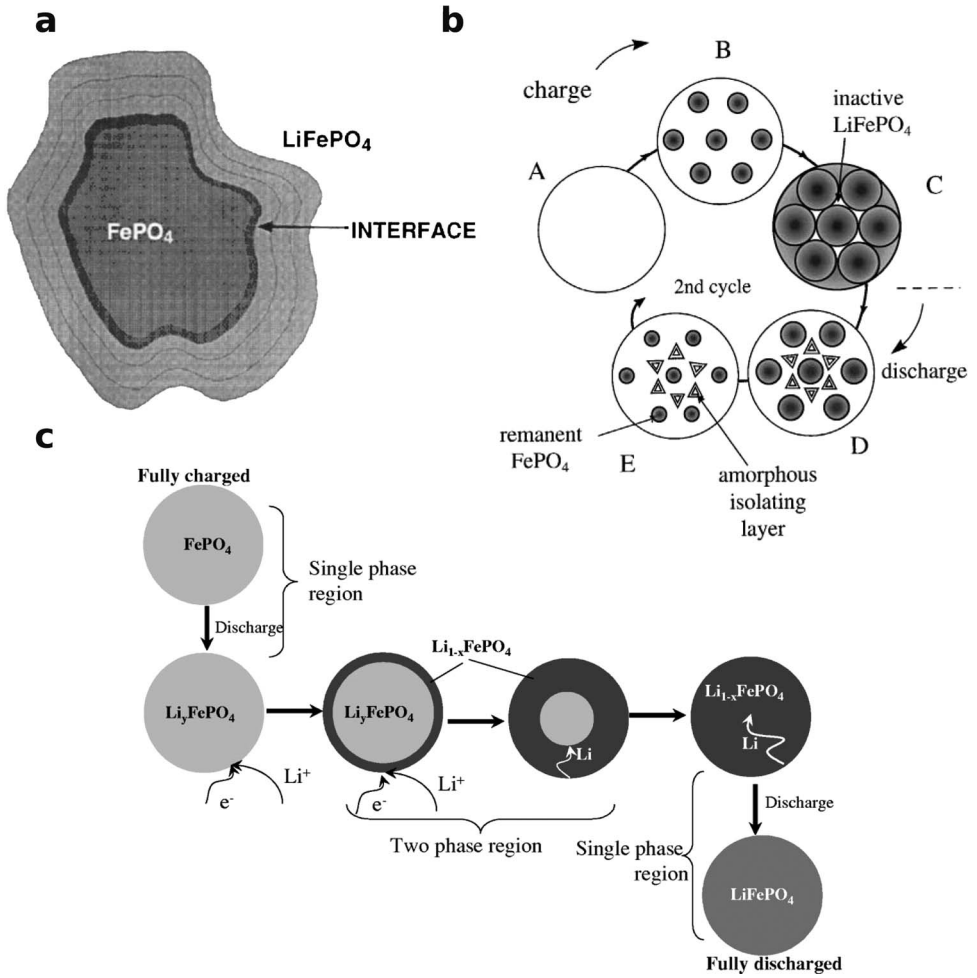

Figure 10. Isotropic models of the single-particle $LiFePO_4$ transformation mechanism as described by (a) Padhi et al.,[1] (b) Andersson et al.,[65] and (c) Srinivasan et al.[122] Reprinted with permission from Ref. 1, copyright 2007, The Electrochemical Society; Ref. 65, copyright 2001, Elsevier; and Ref. 122, copyright 2004, The Electrochemical Society, respectively.

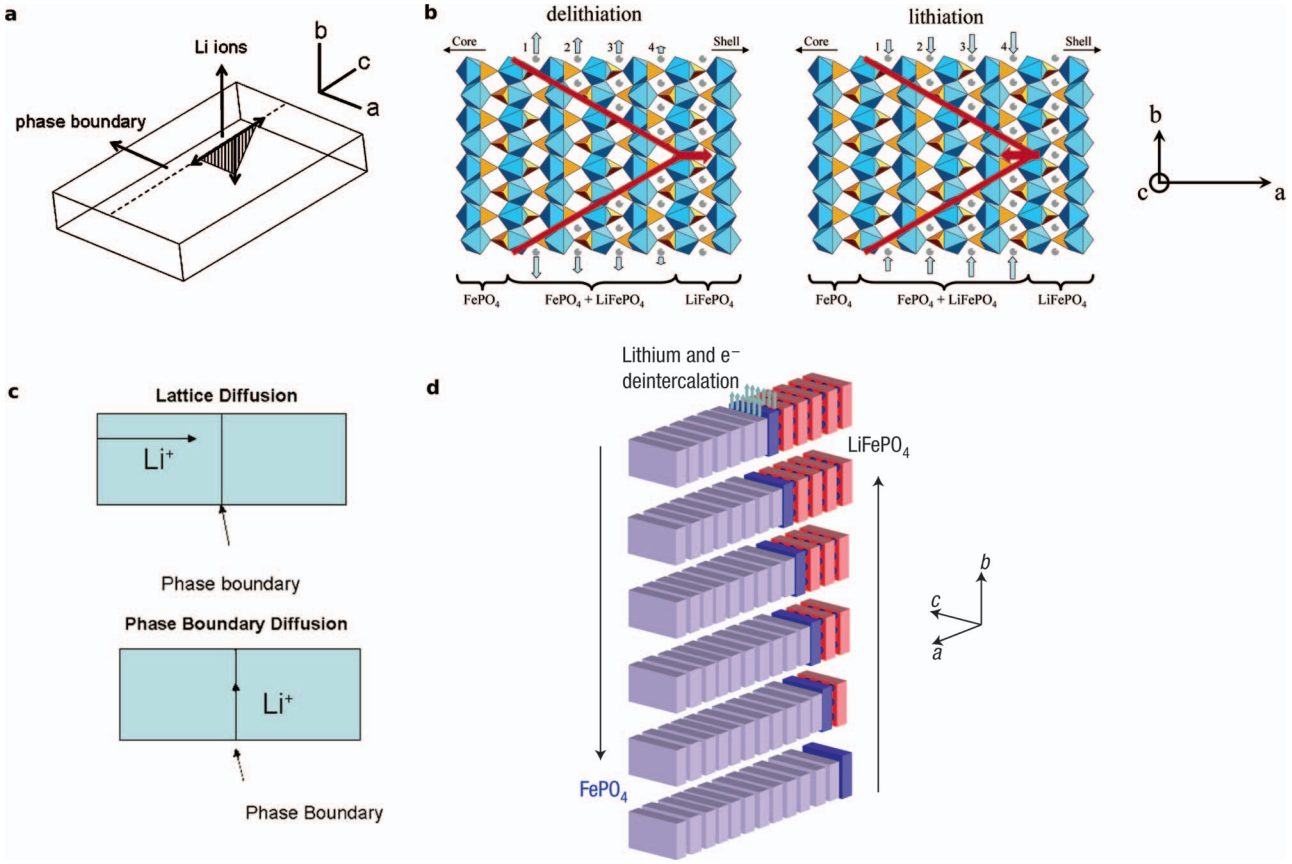

Figure 11. Anisotropic models of the single-particle $LiFePO_4$ transformation mechanism as described by (a) Chen et al.,[28] (b) Laffont et al.,[67] (c) Allen et al.,[75] and (d) Delmas et al.[32] Reprinted from Ref. 28, copyright 2006, The Electrochemical Society; Ref. 67, copyright 2006, The American Chemical Society; Ref. 75, copyright 2008, Springer; and Ref. 32, copyright 2008, Nature Publishing Group, respectively.

certainly limits the efficacy of the initial "core-shell" and "mosaic" models in describing the single-particle lithiation mechanism of functional $LiFePO_4$.

Anisotropic two–phase models: morphology and kinetics.— Given the known Li diffusion and coherency strain anisotropy in $LiFePO_4$, an isotropic "core-shell" mechanism appears both energetically[66] and kinetically unfavorable, prompting Chen et al. to first study the arrangement of Li within a partially chemically delithiated micron-size $LiFePO_4$ particle using HRTEM.[28] The $LiFePO_4/FePO_4$ interface (seen to be ∼4 nm wide) was observed to align preferentially along the *bc* plane (as shown schematically in Figure 11a), the orientation that minimizes the coherency strain energy[24] and maximizes the number of either fully occupied or fully empty 1D Li channels, consistent with rapid Li diffusivity[47] along the [010] direction. Laffont et al. observe similar behavior in partially chemically and electrochemically (ex-situ) delithiated $LiFePO_4$ using both HRTEM and electron energy loss spectroscopy (EELS) and infer a more ordered $LiFePO_4/FePO_4$ interface shown in Figure 11b.[67] Both investigations conclude that the single-particle lithiation mechanism proceeds through a two-phase interface moving perpendicular to the [010] direction as successive *b* channels are emptied on charge and filled on discharge.

The insights gleaned from chemical delithiation experiments, although certainly valuable, cannot substitute exactly for a description of the *electrochemical* lithiation mechanism, and the results from chemical delithiation experiments therefore must be interpreted with the appropriate caveats. Depending on the exact reagents used, the applied driving force for chemical delithiation can be inordinately high,[14] enough to structurally damage the $FePO_4$ host framework, as seen in scanning electron microscopy (SEM) images obtained by Chen et al. displaying noticeable and increasing crack formation in further oxidized samples.[28,68] Introduction of dislocations and cracks during electrochemical Li insertion and deinsertion are well-known causes of increased impedance and capacity fade over time,[69,70] which seems far less likely in nano-$LiFePO_4$ considering the well-observed long cycle life and reversibility at reasonable C-rates typical to conventional battery use. More apparent, the mechanism of combined Li^+ and e^- insertion is fundamentally different in an electrochemical cell than in chemical delithiation. In an electrochemical cell, the Li^+ is incorporated from the electrolyte, and the electron arrives from the current collector; whereas, there is no inherent separation of Li^+ from e^- in the chemical delithiation reaction as illustrated by Weichert et al.[71] Moreover, the final state of a chemical delithiation reaction does not correspond to the same multi-particle equilibrium as earlier discussed, since $LiFePO_4$ particles in solution are not electronically and ionically interconnected to each other. This difference in the defined system constraints in part explains why Delmas et al.[32] observe predominantly fully lithiated and delithiated particles in a partially discharged electrochemical $LiFePO_4$ cell as opposed to intra-particle two-phase coexistence as observed in chemical delithiation experiments. The ionically and electronically well–connected particle network in a real electrode allows the system to access the lower energy states whereby most $LiFePO_4/FePO_4$ interfaces are removed. Hence, it is unlikely that ex-situ observations on chemically delithiated materials bear any resemblance to the intermediate states of charge that an electrode goes through in electrochemical experiments.

The other broad approach employed in the literature to identify the relevant Li insertion and extraction kinetics of Li_xFePO_4 involves analyzing the behavior of a bulk electrode during charge and discharge using conventional electroanalytical methods and, more recently, pairing these methods with in-situ spectroscopy. Potentiostatic charging/discharging experiments performed on a two-phase

system like $LiFePO_4$ can be regarded as an analog to traditional secondary phase precipitation and growth initiated by some constant temperature undercooling. Therefore, traditional phase transformation kinetics models, such as time-cone analysis[72] of concurrent nucleation and growth or Kolmogorov–Johnson-Mehl-Avrami (KJMA) analysis[73] have been used to gain insight into the $LiFePO_4$ phase transformation mechanism.[74–77] By measuring the degree of phase transformation (i.e. the volume fraction of the new phase determined by integrating the current response) with time given a constant applied potential, the dimensionality of the growth mechanism has been interpreted by fitting to the Kolmogorov–Johnson–Mehl–Avrami equation:

$$f = 1 - \exp(-kt^n) \quad [4]$$

where f is the volume fraction of the secondary phase, t is the transformation time, and k and n are fitting parameters. The information describing the phase transformation mechanism is contained in n, the Avrami exponent, which can range from values of ∼1 to 4, with lower values signifying a 1D growth mechanism ($n \sim 1$–2) and higher values signifying either 2D ($n \sim 2$–3) or 3D ($n \sim 3$–4) growth. Hong et al. find $n = 1.6$ charging ∼1 μm aggregates of $Li_xFe_{0.9}Mg_{0.1}PO_4$ with a potential step from 3.1 to 3.48 V (with respect to Li metal).[74] Allen et al. determine $n \sim 1$ in 60–70 nm $LiFePO_4$ particles discharged from 4.2 to 3.0 V,[78] and more recently, Oyama et al. find $n = 0.66$ and $n = 1.08$ in 203 nm $LiFePO_4$ particles discharged from 3.5 to 3.35 V and 3.42 to 3.41 V, respectively.[77] Also, in the work by Oyama et al., the data obtained from charging and discharging smaller particles (84 nm and 45 nm) could not be fit to the Avrami equation with $n \geq 1$. All of these results are seemingly at odds with the initial proposed isotropic growth models (shown in Figure 10), which conform to 3D growth (and would therefore result in n ∼2–3), and alternatively support the existence of anisotropic growth. The Avrami exponent n also contains information on possible rate-limiting kinetic transformation mechanisms:

$$n = a + bc \quad [5]$$

where a indicates the rate behavior of nucleation, b refers to the dimensionality of growth, and c describes the rate of growth. The possible values of a, b, and c, as well as their physical significance are shown below in Table I.[79] Allen et al. initially interpreted $n \sim 1$ as a 1D constant growth mechanism, informed by anisotropic diffusion of Li within $LiFePO_4$, with zero nucleation rate (i.e. $a = 0$, $b = 1$, and $c = 1$),[78] and then later revised the model noting that a 1D diffusion mechanism can facilitate 2D diffusion-controlled phase boundary growth with zero nucleation rate (i.e. $a = 0$, $b = 2$, and $c = 1/2$),[75] to better agreement with the models proposed by Chen et al. and Laffont et al. Both of these descriptions of the phase transformation mechanism are highlighted in Figure 11c.

As with chemical delithiation experiments, special attention should be paid to the applicability of KJMA analysis to exactly describing the lithiation kinetics of phase transformation electrodes by examining the strength of the model's inherent assumptions. The KJMA equation was initially derived to describe an isothermal phase transition in a bulk material (i.e. crystallization from melt) rather than a phase transformation propagating through an assembly of many discrete small particles (like in a Li_xFePO_4 electrode).[80] In the latter case, the assumption of homogeneous nucleation may be tenuous considering the increased availability of surface nucleation sites with small particles. Also, the critical nuclei may approach the size of the active $LiFePO_4$ particles themselves, especially at low overpotential, which makes the built–in assumption of a zero–volume critical nucleus size problematic. The overall transformation behavior described by the KJMA equation corresponds to initial slow transformation rate with the first nucleation of the second phase, then rapid growth of nuclei unimpeded by each other, and again reduced rate of transformation due to growing nuclei impinging on each other. In a multi-particle system, however, no single growing nucleus can exceed the size of its host particle, an important constraint not considered in the initial KJMA formulation, which far decreases the likelihood of growing $LiFePO_4$ grains impinging on each other, and is only exaggerated in a system of consisting of nano-size $LiFePO_4$ particles. Also, when applying large potential steps to initiate phase-transformation, the spatial gradient of the potential across the cell is likely very sharp and non-uniform, and will vary depending on the electrode architecture (loading density, thickness, etc.), meaning that the driving force for transformation may vary drastically within the electrode itself. To this end, the accuracy of KJMA analysis increases in systems with larger particle size and homogeneous distribution of the applied potential across the cell, to qualitative agreement with the measurements performed by Oyama et al.[77] who find more amenable values of the Avrami exponent consistent with nucleation and growth ($n \geq 1$) in larger particles (203 nm) with small applied overpotential (10 mV steps).

Noting the importance of analyzing electrochemically discharged and charged particles to gain insight into the single-particle transformation mechanism, Delmas et al. characterized several partially electrochemically delithiated Li_xFePO_4 samples with varied average Li concentration using ex-situ XRD.[32] Interestingly, the XRD spectra exhibit no peak shifting or broadening with changing average Li concentration, and rather appear as a linear combination of the $LiFePO_4$ and $FePO_4$ spectra superimposed on each other. This corresponds to a state where a fraction of the active $LiFePO_4$ particles are fully lithiated, and the remainder fully delithiated, and has recently been confirmed directly using TEM equipped with precession electron diffraction (PED) phase-mapping capability.[33] As discussed earlier, this arrangement well describes the equilibrium defined by an electronically and ionically interconnected network of particles, each with non-convex free energy with respect to Li concentration. The lingering question shifts to determining whether this final state is simply the result of the system equilibrating ex-situ, or actually describes a particle-by-particle kinetic (de)lithiation mechanism. Assuming the latter, Delmas et al. have proposed the "domino-cascade" model, where phase-boundary propagation perpendicular to the b axis is extremely rapid compared to initial nucleation (Figure 11d), meaning that at any given snapshot in time a Li_xFePO_4 particle is most likely to be either fully lithiated or delithiated, effectively rationalizing their results.

To this point, even with the progress made in understanding the possible single-particle lithiation mechanisms, the origin of the exceedingly rapid charging and discharging capability of $LiFePO_4$ (especially in comparison to Li intercalation systems without strong first-order phase separating behavior) has remained unaddressed. Inherent to a two-phase growth mechanism, the basis for all mechanisms discussed thus far, is a nucleation step followed by two-phase growth. A single–phase mechanism, however, avoids the additional kinetic barriers associated with nucleation and growth altogether, and the barrier for nucleation as estimated from classical nucleation theory is not insignificant. Considering the discharge (lithiation) process, Li ions coalesce together within the $FePO_4$ framework with some applied driving force (underpotential). Whether growth continues or not

Table I. Values and corresponding physical meaning of geometric and kinetic growth parameters of the Avrami exponent as defined in Equation 5.

Parameter Value	Physical Meaning
a = 0	Zero nucleation rate
a = 1	Constant nucleation rate
a > 1	Increasing nucleation rate
0 < a < 1	Decreasing nucleation rate
b = 1	1D growth mechanism (i.e. needle)
b = 2	2D growth mechanism (i.e. disk)
b = 3	3D growth mechanism (i.e. sphere)
c = 1	Linear phase boundary growth (i.e. phase-boundary limited growth)
c = 1/2	Parabolic phase boundary growth (i.e. diffusion-limited growth)

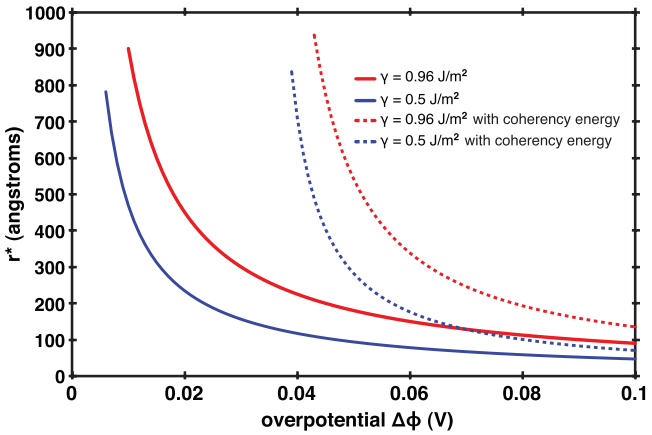

Figure 12. Plot of critical nucleus size (r*) vs. overpotential ($\Delta\Phi$) related by equation 7 including and not including coherency energy[24] (dashed and solid lines, respectively), for different values of the $LiFePO_4/FePO_4$ interfacial energy γ (0.96 J/m^2, in red, from literature[25] and 0.5 J/m^2, in blue).

depends on if the bulk free energy reduction from creating a $LiFePO_4$ cluster outweighs the positive energy penalty associated with creating a coherent $LiFePO_4/FePO_4$ interface. Only beyond some critical nucleus size does growth become stable, and only with greater applied driving force can the critical nucleus become smaller. Assuming isotropic interfacial energies and coherency strain, the critical nucleus size (of radius r^*) and critical nucleus barrier (G^*) can be roughly estimated using well–known expressions derived from classical nucleation theory:

$$\Delta G_{r^*} = \frac{16\pi \cdot \gamma^3 \cdot v^2}{3(|\Delta\phi| - \Delta g_s)^2} \quad [6]$$

$$r^* = \frac{2 \cdot \gamma \cdot v}{(|\Delta\phi| - \Delta g_s)} \quad [7]$$

where γ is the $LiFePO_4/FePO_4$ interfacial energy, υ is the molar volume of $LiFePO_4$, Δg_s is the coherency strain energy, and $\Delta\phi$ is the applied potential. The variation of the critical nucleus size with applied potential according to 7 is shown in Figure 12 using values for γ, υ, Δg_s obtained from the literature.[24,25] Even by approximately accounting for heterogeneous nucleation by ignoring the coherency strain energy altogether ($\Delta g_s \sim$ 3,200 J/mol or 33 meV/Li for an interface oriented along the *bc* plane)[24] and considering only half of the interfacial energy obtained from literature (i.e. one half of γ = 0.96 J/m^2),[25] a 50 nm critical nucleus, which is also the typical size of an entire nano–$LiFePO_4$ particle, requires in excess of 50 mV underpotential (as shown by the solid blue line in Figure 12) with G_{r^*} approaching several hundred thousand kT (thermal energy) per nucleus cluster at room temperature. The plot shown in Figure 12 conveys an overarching point: the minimum ~10–20 mV (under)overpotential required for complete (dis)charge[31] observed in experiments is unusually small and a lithiation mechanism contingent on a nucleation step cannot account for this. This analysis motivates the possibility that the single-particle phase transformation in $LiFePO_4$ may avoid crystalline nucleation and growth and veer from the equilibrium phase diagram. Instead, the transformation, especially in nano-particles, likely occurs through an alternative non-equilibrium pathway that may be energetically costlier, but kinetically faster. Also, the characteristic feature of the open–circuit voltage curve, namely the plateau at ~3.4 V for the bulk of the Li concentration range, can still be accounted for by considering the equilibrium defined by a system of multiple $LiFePO_4$ particles, each with a non-convex free energy conforming to the particular transformation path in consideration (as discussed in 2.3 and 3.2.3 and illustrated in Figure 7g).

Dynamic amorphization.— Meethong et al.[35] investigated the possible formation of an amorphous phase stabilized at the active particle surface which may assist the phase transformation kinetics, and Tang et al.[81,82] later investigated the conditions (applied potential, particle size, misfit strain, etc.) where such a mechanism is likely to be predominant using a diffuse-interface continuum model. An amorphous transformation scheme offers several kinetic advantages over the traditional crystalline nucleation and growth mechanism. Although the volume free energy is higher compared to the bulk 2-phase $LiFePO_4/FePO_4$ equilibrium, formation of an amorphous phase ensures that the surface energy is likely lower, crystal–glass interfacial energy is likely lower, and misfit stresses are better relieved, which overall implies faster nucleation kinetics.[83] In addition to improved nucleation kinetics, ceramic glasses are known to be fast isotropic ionic conductors, which may offer improvement over 1D diffusion in crystalline $LiFePO_4$ and accelerate growth. Through analysis of the intensity of both $LiFePO_4$ and $FePO_4$ peaks in in-situ XRD spectra captured at different state of charge (at C/50 rate in 34 nm particles), Meethong et al. determine the relative phase fraction of each phase. Unexpectedly, the phase fraction was observed to vary non-linearly with state of charge, which was thus interpreted as proof of the formation of an amorphous phase to ensure mass balance.[35]

Amorphization provides a compelling explanation for fast (de)lithiation kinetics in Li_xFePO_4, but there are some unresolved questions which give pause for further consideration. Presumably, the initial and final states are still both crystalline (either olivine $FePO_4$ or $LiFePO_4$), meaning that in addition to nucleating an amorphous phase, there is also a recrystallization process, which will undoubtedly have its own additional kinetic barriers. Also in the case of charging, the amorphous phase must recrystallize into metastable olivine $FePO_4$, rather than into the equilibrium berlinite crystal structure.[84] If, however, there is no recrystallization and the amorphous structure is retained, it is especially surprising that this process would occur at or near the identical potential as the $LiFePO_4/FePO_4$ crystalline phase transformation (~3.5 V vs. Li). Considering a crystalline to amorphous transformation path from an atomistic point of view, significant bond breaking and rotation must occur, which intuitively seem more kinetically burdensome than Li insertion into a purely crystalline intercalation structure, especially surprising given the apparent less–than ~50 mV overpotential required to initiate the transition as observed by Meethong et al.[35] From an experimental methods standpoint, confirmation of the existence of an amorphous phase purely from XRD peak intensities has been recently questioned,[85,86] owing to disagreement over the cause of the so-called "delay" observed in in-situ experiments which may be the result purely from electrode-scale inhomogeneity enhanced by pressure gradients in the electrode.[86] Nevertheless, consideration of a potential amorphous transition path helps clarify the necessary overall criteria for any realistic $LiFePO_4$ single-particle non-equilibrium lithiation model: 1) an expedient kinetic (de)lithiation mechanism that is 2) available with small (~10–20 mV) driving force.

Non-equilibrium solid-solution transformation.— A phase transformation mechanism that traverses entirely through the non-equilibrium solid-solution phase satisfies both criteria (rapid intercalation kinetics available with little driving force), as illustrated by the free energy curve and atomic configurations depicted in Figure 3a and Figure 3b. By definition, a continuous and reversible transformation path through the solid-solution *must* exist since the start and end states (either $LiFePO_4$ or $FePO_4$) are topotactically related, and the kinetic advantages are readily apparent. The salient aspects of Li insertion via the non-equilibrium solid-solution pathway as compared to the standard nucleation and growth model are illustrated schematically in Figure 13. Not only does a solid-solution transformation mechanism avoid the significant energy barrier associated with nucleation as earlier discussed, but also every *b* channel, which facilitates fast Li diffusion, is active in either taking up or removing Li compared to the anisotropic two-phase growth mechanisms where Li can be incorporated strictly at the $LiFePO_4/FePO_4$ interface.

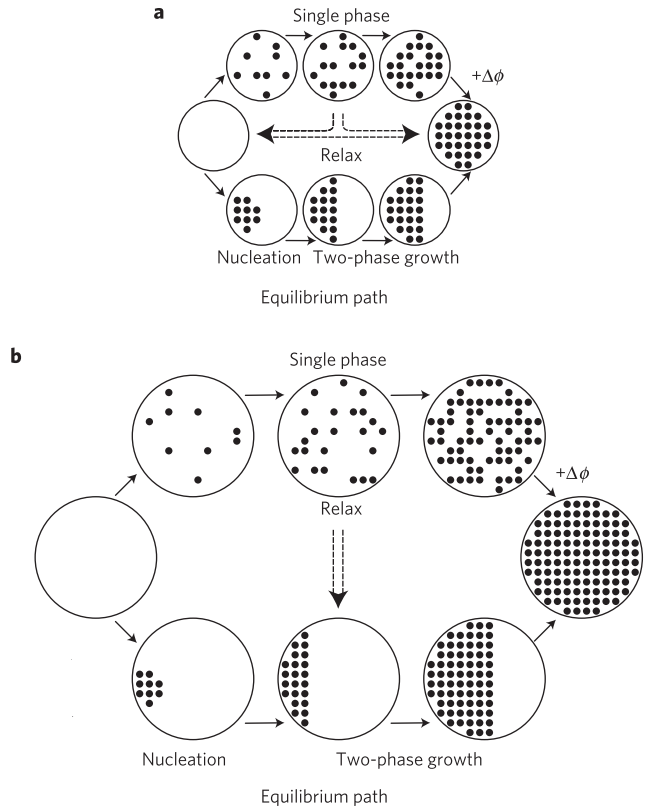

Figure 13. Comparison of equilibrium and non-equilibrium lithiation in $LiFePO_4$. a,b, Schematic depiction of lithiation via an equilibrium two-phase path (bottom path) characterized by nucleation and growth compared with an alternative non-equilibrium single phase path (upper path) enabled by underpotential $\Delta\Phi$ shown for small particles (a) and larger particles (b). Once the underpotential is removed the system relaxes to the equilibrium state.

Whether this proposed lithiation mechanism is practically feasible or not depends on the driving force required to access the solid-solution state. Fortunately, as determined from first-principles and shown in Figure 3a, the free-energy of mixing is unusually low, less than ∼15 meV per formula unit at all Li concentrations at room temperature and well below kT (∼26 meV at room temperature).[19] Considering that batteries are potential–controlled systems, it is more instructive to consider the overpotential (or underpotential) $\Delta\phi$ required to charge (or discharge) via the solid-solution pathway, which can be obtained from the instantaneous slope of the mixing free energy ΔG with Li concentration x_{Li}:

$$\Delta\phi = -\Delta\mu_{\mathrm{Li}} = -\left(\frac{\partial \Delta G}{\partial x_{\mathrm{Li}}}\right)_T. \qquad [8]$$

Qualitatively, the single-particle potential curve obtained from 8 resembles that shown schematically in Figure 7, with only ∼30 mV separating the charge and discharge plateaus (as shown in Figure 7g), to excellent agreement with the experiments performed by Dreyer et al. who observe a ∼20 mV voltage hysteresis between charge and discharge in the zero-current limit (C/1000).[31]

In general, a non-equilibrium solid-solution transformation will have substantially different kinetic behavior than an equilibrium solid-solution mechanism even though both proceed through a single phase. The source of this varied behavior is the shape of the single-particle Li chemical potential, which increases monotonically with Li content in the equilibrium scenario (shown schematically in Figure 5a) compared to the non-equilibrium case (Figure 5b). In a hypothetical system where the solid-solution is thermodynamically stable at all Li concentrations, the driving force for further Li removal upon charging continually decreases given some fixed positive applied potential. Now consider charging a single $LiFePO_4$ nanoparticle through the non-equilibrium solid solution path. After exceeding some critical overpotential (only ∼10 mV as determined from first-principles calculations[19]) the driving force for additional Li removal actually initially increases and enables complete delithiation. Given the rapid transport of Li in $LiFePO_4$ nanoparticles, this mechanism rationalizes the overall facile transformation kinetics and enhanced rate performance observed in nano-$LiFePO_4$ electrodes. If the applied potential is removed mid-charge, again the behavior differs between the equilibrium and non-equilibrium scenarios. In the former case, the Li will always homogenize within the particle; whereas in the latter case, the system will relax to the equilibrium phase-separated state (shown in Figure 13), either two-phase coexistence within the same particle or inter-particle two-phase coexistence in a multi-particle system (as described in detail in the Multi-Particle Equilibrium section). Which of these two phase-separated states (inter– or intra–particle) occurs will depend on the particle size and the inter–particle transport characteristics.

When the mixing free energy is concave with respect to Li content, that is $\left(\frac{\partial^2 \Delta G}{\partial x_{Li}^2}\right) < 0$, local Li concentration fluctuations can spontaneously induce continuous phase separation, a process known as spinodal decomposition and well-described at the continuum scale by the Cahn-Hilliard equation.[72] Physical solutions to the Cahn–Hilliard equation in systems with fixed concentration are stripes or lamellae of alternating equilibrium composition, the width of which are determined by the $LiFePO_4/FePO_4$ interfacial energy and coherency strain energy. In an open system, however, there is no precondition to dynamically form such structures as any penalty associated with creating a coherent interface can be avoided by either removing or adding Li to the system, which eventually evolves toward a single equilibrium composition. Nevertheless, there is still some driving force to dynamically phase separate during the single-particle charging and discharging process arising from the concavity of the free energy, but as seen from the free energy curve in Figure 3a, the single-phase Li_xFePO_4 free energy is almost entirely flat for the entire Li concentration range,[19] meaning that this driving force is likely not significant. Bai et al. have established a general methodology that accounts for the dynamic phase separation during the charging and discharging process.[87] Specifically, they constructed a phase-field model using a regular solution uniform free energy density coupled to a modified Butler-Volmer equation for galvanostatic Li insertion or removal at the particle surface, and also assume rate-limiting surface-transfer kinetics, anisotropic Li transport (i.e. fast 1D diffusion), and uniform Li^+ concentration in the electrolyte. Interestingly, above a critical current, the rate of phase decomposition is overwhelmed by the rate of Li insertion or removal creating a "quasi-solid solution" state, and at even higher currents, there are no stable solutions that involve phase separation.[87]

With increasing particle size, however, Li insertion becomes transport–limited in the large–particle limit, and the rate of phase separation undoubtedly outpaces solid–solution based insertion simply because Li must travel much further within the particle to homogenize. Thus, there is some critical particle size above which a two-phase growth mechanism occurs and below which a single-phase transformation path is favored. It is therefore the combined benefit of both unblocked fast 1D diffusion channels and favored solid-solution transformation that makes rapid charging and discharging more amenable in nano-$LiFePO_4$ particles compared to larger particles.

Since the outset of $LiFePO_4$ research in 1997, characterizing the single-particle lithiation mechanism has been itself an open and active area of study within the field, and for good reason. The key to identifying the origin of the now well-known rapid rate performance of $LiFePO_4$ despite its equilibrium phase-separating behavior lies in the careful analysis of the single-particle mechanism. Over the years, a variety of different single-particle models with their notable features have been proposed: isotropic two-phase growth, anisotropic two-phase growth, dynamic amorphization, and most recently non-equilibrium solid-solution transformation. Of these models, the solid-

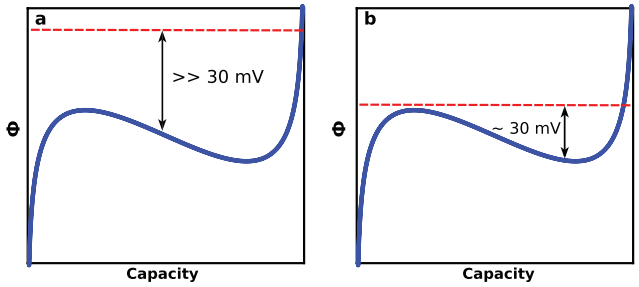

Figure 14. Schematic representation of charging at high (a) and low (b) rate. The driving force for Li removal is represented by the difference between the applied potential Φ_{app} (dashed red) and the single-particle potential (solid blue).

solution mechanism appears especially appealing as it convincingly explains the unusually rapid Li insertion kinetics accessible with little overpotential (∼10–20 mV) as observed experimentally. Although most of the $LiFePO_4$ literature has focused on clarifying the single-particle mechanism, the existence of a non-equilibrium transformation path ensures that the multi-particle kinetics at the electrode scale are non-trivial and itself a subject that merits further investigation.

Electrode-scale (de)lithiation.— An implicit assumption in the traditional analysis of experimentally obtained charging and discharging data involves the single-particle behavior mirroring the electrode-scale behavior. This assumption is what enables materials properties such as Li diffusivity and insights regarding the single-particle lithiation mechanism to be extracted from conventional electrochemical experiments. The Li_xFePO_4 multi-particle equilibrium (discussed in detail in a previous section), however, exhibits a large degree of inhomogeneity at any intermediate state of charge with some particles fully lithiated and the remaining fraction fully delithiated. In the quasi-static limit, an assembly of $LiFePO_4$ particles will charge sequentially[31] rather than in parallel as assumed in conventional electrode-scale models as a consequence of the unusual shape of the single-particle potential.

Now consider the opposite scenario, charging an assembly of $LiFePO_4$ particles by applying a very large constant overpotential (i.e. $\Delta\phi \gg 30$ mV, well in excess of the zero-current voltage gap[31]) and tentatively assume there are no rate limitations stemming from either Li^+ salt depletion in the electrolyte or poor electronic transport from the current collector. In this hypothetical limit, the large applied potential is far greater than the scale of the features of the single-particle potential curve, meaning that the driving force (i.e. the difference between the applied potential and single-particle potential) for Li removal from any and every $LiFePO_4$ particle in the system is roughly the same as illustrated in Figure 14a compared to Figure 14b. Consequently, all particles charge simultaneously and in parallel in the large overpotential limit idealized scenario. Therefore, at intermediate charging rates, the multi-particle behavior is much more complex and lies somewhere in the middle, with some combination of particles charging in parallel and in series.

Intuitively, it is much more efficient to charge all particles within an electrode in parallel rather than one-by-one. To draw a fixed current, charging in sequence requires each particle, locally charged at an exceedingly high rate, to sustain all of the power in the electrode. In the converse scenario where all particles charged in parallel, however, the current is distributed equally amongst all particles, which are charged simultaneously each at a much lower relative rate. The notion of more effective power distribution at higher rates is a curious outcome, but one that is predicated upon rapid electrode-scale kinetics and uniform distribution of the potential across the cell. Practically, this implies that cell construction and architecture play critical roles to access $LiFePO_4$'s full rate capability, and indeed, noticeable empirical improvements in cell rate performance have been achieved through electrode-level modifications: most notably through adding carbon,[4] synthesizing $LiFePO_4$ nano-particles with Li conducting amorphous coating,[7] varying the electrode thickness,[46] and diluting the active mass (with inactive material) of the electrode.[6]

Carbon coating.— Ravet et al. first observed the benefits of carbon-coating,[4] observing peak sharpening in cyclic voltammetry data and overall enhancement of cycling kinetics and stability. Incorporating carbon coatings has now become one of the most common strategies to improve the rate performance of not only $LiFePO_4$ electrodes, but other chemistries as well.[88] An elaborate survey of the use of carbon-coatings and other sources of carbon addition in $LiFePO_4$ electrodes has been assembled and published elsewhere, with significant detail paid to different synthesis methods and the general impact on experimental performance.[89] Overall, any improvement in the charge and discharge kinetics as a result of carbon addition cannot come from improving the bulk transport within the active material, specifically the bulk electronic conductivity. Rather, carbon addition primarily improves the electronic contact between active particles and improves electronic connectivity to the current collector which makes for more effective current distribution at intermediate rate. Alternatively, another area of kinetic improvement may come indirectly from the simultaneous restriction of active particle growth to the nano-scale with carbon-coating formation in the synthesis process arising from the decomposition of organic precursors.[90] In fact, this may be the most compelling explanation as pointed out by Gaberscek et al. in a survey of published electrochemical data comparing the per-

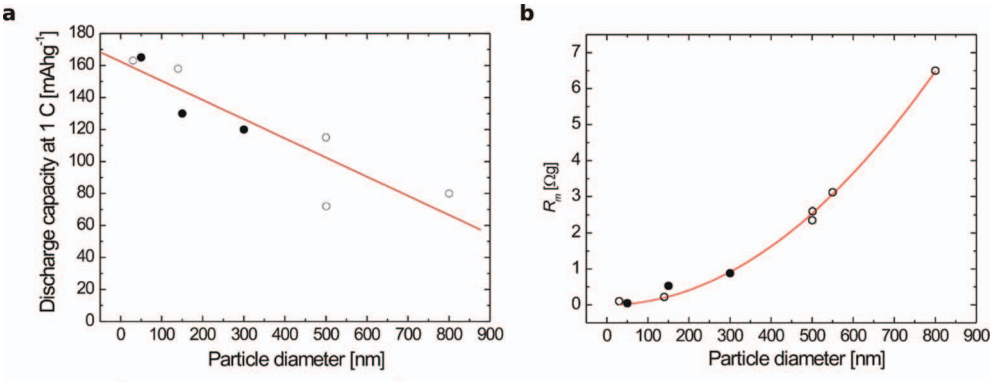

Figure 15. (a) Discharge capacity at 1C rate vs. particle diameter with carbon-coating/added carbon black (black circles) and without (hollow circles), along with linear regression fit (red). (b) Electrode resistance per mass R_m vs. particle diameter with and without carbon addition (black and hollow circles, respectively), along with power law fit (red). All data obtained from the literature as collected and assembled by Gaberscek et al.[91] Reprinted with permission from Ref. 91, copyright 2007, Elsevier.

formance of carbon-coated $LiFePO_4$ to non-carbon-coated $LiFePO_4$ which concluded that improved rate performance is highly correlated with smaller active particle size rather than the presence of carbon coating as clearly seen in Figure 15.[91] Also, the presence of a collection of $LiFePO_4$ nanoparticles embedded in a carbon matrix allows for additional mechanical stability, better accommodating the sizeable active particle volume change upon Li insertion and deinsertion.[90]

Ionically conductive coatings.— In addition to synthesizing nano-$LiFePO_4$ particles with carbon-coating, the best rate performance achieved to date in a lab setting, accessing nearly two thirds of the theoretical capacity at ∼200 C and about 1/3rd of the capacity at ∼400 C, has been through charging and discharging $LiFePO_4$ nanoparticles (∼50 nm) synthesized with poorly crystallized rapid ionic conducting glass-coatings.[7] A novel synthesis technique, intentionally steering the off-stoichiometry toward $LiFe_{0.9}P_{0.95}O_{4-\delta}$, results in the formation of an amorphous coating surrounding the active $LiFePO_4$ particles with a self-limited thickness comprising of most likely a combination of Li_3PO_4 and $Li_4P_2O_7$ as predicted by the first-principles determined phase diagram.[92] The purported mechanism of improved kinetics here is not only enhanced Li mobility within the glassy layer but also potentially improved surface Li incorporation kinetics between the electrolyte and surface coating. Adams et al., using a bond-valence force field method, calculated a 3 order of magnitude increase in the surface ionic conductivity with a $Li_4P_2O_7$ particle coating, which supports the former assertion.[93] As with carbon-coated particles, the benefit of ionically conductive glassy coatings does not lie in assisting the Li intercalation kinetics *within* the active particle itself, but rather in improving the kinetics of transporting Li *to* the active particle.

Electrode thickness and dilution.— Along the same lines of altering the electrode architecture to improve overall electrode kinetics, the rate performance can be enhanced by varying the electrode thickness and also diluting the concentration of active mass (with inactive material). Gaberscek et al. specifically studied the impact of optimizing the electrode "wiring," that is the ionic and electronic connectivity between particles and also to the electron and Li^+ source (i.e. current collector and electrolyte, respectively). In particular, they systematically monitored the variation of reversible capacity and polarization as a function of both electrode mass and charge/discharge rate, while keeping the remaining parameters (i.e. particle size, porosity, etc.) as close to constant as possible. Interestingly, at low currents the kinetics are limited by the active particles themselves, supported by the non-linear behavior of current with polarization (roughly resembling Butler-Volmer behavior), and at higher rates, the rate limitation comes purely from the electrode resistance, corroborated by the linear increase of the polarization with current (as shown in Figure 16a, this given constant electrode mass/thickness). At low rates (ranging from C/20 to 1C), the reversible capacity remains nearly unchanged with electrode thickness, but at higher rates (ranging from 1C to 20C) there is a sharp decline in the reversible capacity with increasing thickness. This supports the notion that at higher rates, the rate-limiting step is no longer intercalation of Li within the active particles, but the passage of electrons and Li^+ through the electrode. The result is somewhat surprising, considering that much of the $LiFePO_4$ literature assumes that Li insertion into Li_xFePO_4 is inherently slow (either due to poor bulk electronic or ionic conductivity) and therefore is likely rate-limiting in all charging and discharging conditions (both low and high rate), certainly in comparison to Li^+ transport through the electrolyte and electron transport through carbon. Liu et al. were able to visualize the distribution of $LiFePO_4$ and $FePO_4$ spatially along directions parallel and perpendicular to the current collector within a thick electrode (40 mm by 45 mm) at intermediate states of charge using synchotron X-ray microdiffraction.[94] After charging to 50% state of charge at low rate (∼0.11 C) the $FePO_4$ distribution is nearly uniform throughout the cell, and after charging at much higher rate (∼18 C) the $FePO_4$ distribution is much more inhomogeneous, specifically in the direction perpendicular to the current collector. Again, this finding suggests that at high rates, the transport of either Li^+ or e^- to the active material is rate-limiting and points to unconventional multi-particle behavior that manifests itself by varying the electrode dimensions.

Another method to improve the electrode-scale kinetics involves diluting the active mass with electrochemically inactive material. For example, Johns et al. constructed composite electrodes with commercially synthesized $LiFePO_4$, acetylene black, TiO_2 (anatase), and PVDF binder with varying concentrations. Specifically, keeping the overall concentration of acetylene black and binder constant, sample

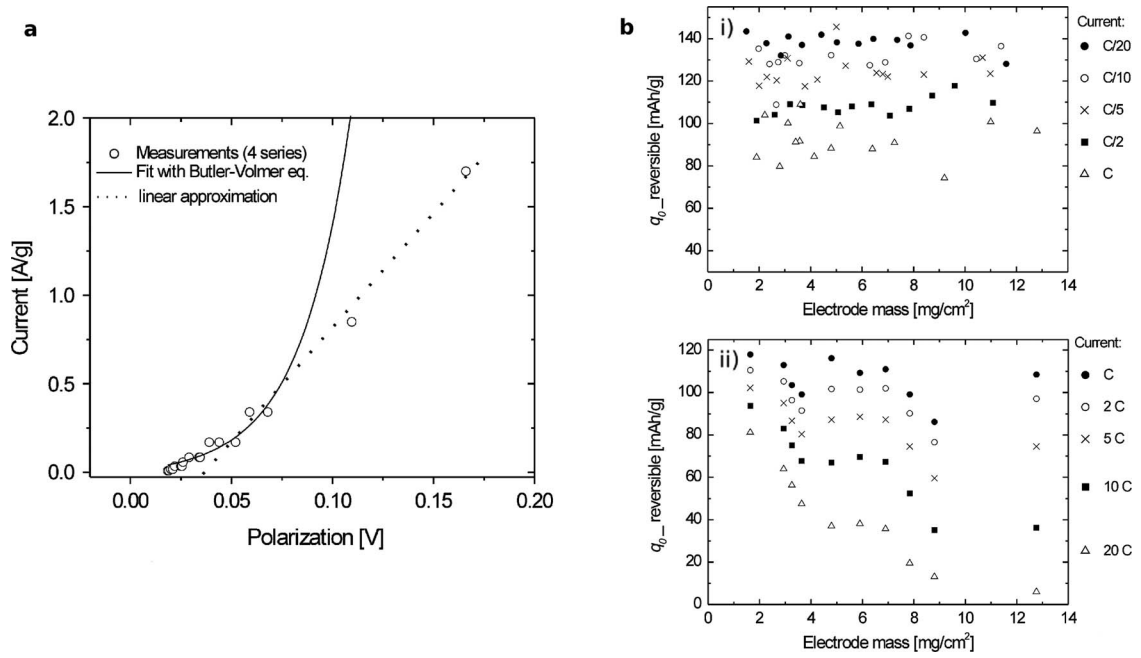

Figure 16. (a) Galvanostatic current (circles) plotted against polarization voltage, performed on 4 different electrodes having comparable mass (5–7 mg) as determined by Gaberscek et al.[46] (b) Reversible charge capacity plotted against electrode mass (thickness) at different rate as determined by Gaberscek et al.[46] Reproduced with permission from Ref. 46, copyright 2007, PCCP Owner Societies.

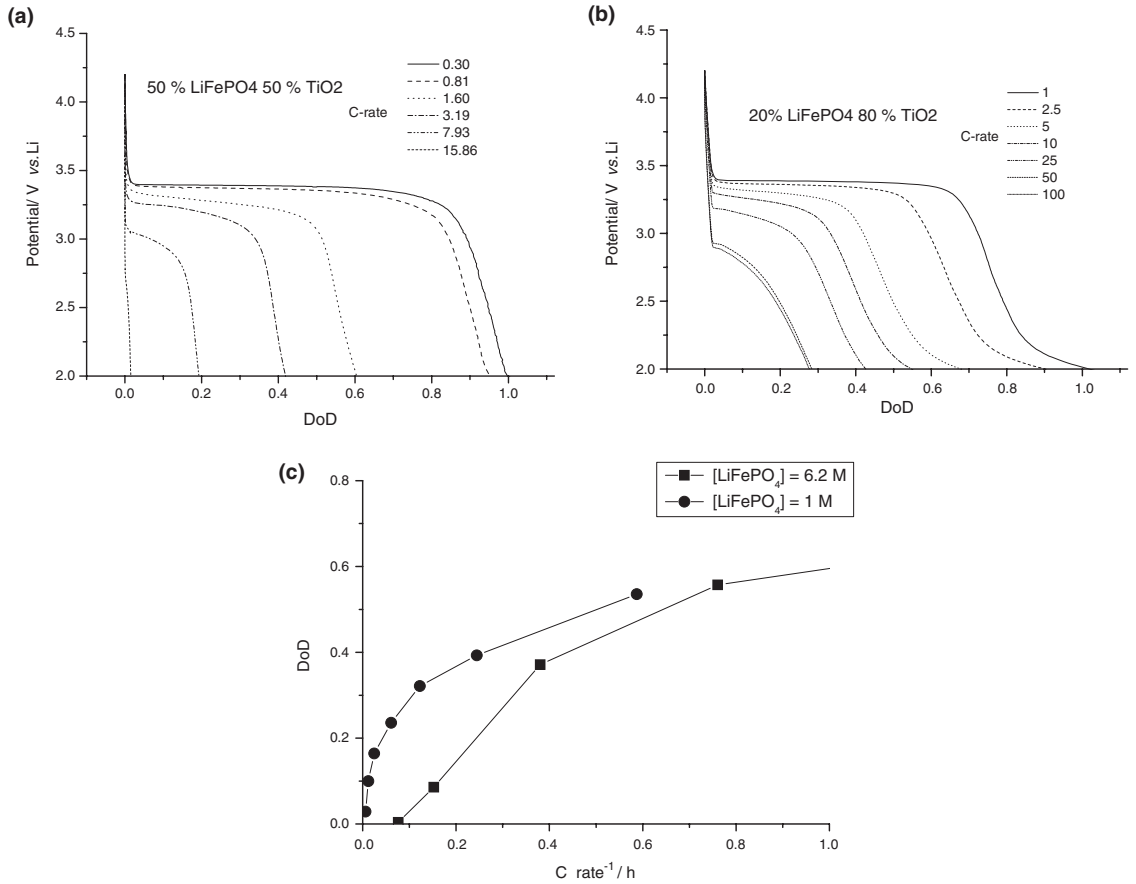

Figure 17. (a) and (b) Discharge curves for $LiFePO_4$ showing rate enhancement on dilution with TiO_2. (c) Depth of discharge (DoD) vs. rate^{-1} for two active material dilutions 80:20 (6.2 M) and 20:80 (1 M) in the composite electrode as performed and collected by Johns et al.[6] Reprinted with permission from Ref. 6, copyright 2009, Elsevier.

electrodes were assembled with decreasing concentrations of $LiFePO_4$ offset by increasing concentrations of TiO_2, which is electrochemically inactive in the typical $LiFePO_4$ cycling window. Samples with increased dilution (i.e. more $LiFePO_4$ substituted with TiO_2) exhibit far superior rate-performance especially at high rates, highlighted in Figure 17, which in itself illustrates that the source of rate limitation in this regime is the electrode construction rather than Li intercalation into active single particles.[6] By diluting the electrode and constructing a simple yet powerful model of Li diffusion across the electrode, Johns et al. identified that at high charging and discharging rates, the concentration of Li salt in the electrolyte is locally depleted which limits the accessible capacity but is mitigated by reducing the overall content of $LiFePO_4$ within the electrode.

Electrode-scale inhomogeneity.— Beyond reducing the particle size to nano-dimensions, all of the major developments to enhance the high-rate performance of $LiFePO_4$ electrodes have historically been the result of electrode-scale improvements. Moreover, these apparently different strategies (carbon coating, ionically conducting coatings, modified electrode thickness, and electrode dilution) hinge on the same principle. In effect, they all seek to optimize the "electrode wiring" and homogenize the distribution of the applied electrochemical potential across the cell, which is required to access the inherent high rate capability of $LiFePO_4$. Although the aforementioned modifications are performed at the electrode-scale, they facilitate the entire assembly of active particles to charge and discharge differently as a whole, a phenomenon that is unique to phase-transformation electrode materials (due to the characteristic non-monotone single-particle potential). Consider a "less-than-ideal" wired electrode, where the electrochemical potential is inhomogeneously distributed due to poor and varying ionic electronic connectivity throughout the cell. Although this cell construction will result in overall poorer performance for any given electrode material (two-phase or otherwise), the deleterious effects are exacerbated in $LiFePO_4$ electrodes. Those particles that are best "wired" experience the greatest electrochemical driving force for transformation. Therefore, they first undergo complete phase transformation and sustain the entire current demands of the cell, overall resulting in an inefficient sequential particle-by-particle charging/discharging scheme, in this case even at finite current conditions. In a worst-case scenario, the local Li availability (on discharge for instance) in the electrolyte is depleted or electronic connection to the counter-electrode is so poor such that the most kinetically expedient method of intercalation comes via inter-particle transport (implying simultaneous charging and discharging within the same cell).

The electrode-scale inhomogeneity in $LiFePO_4$ electrodes during charging and discharging is no more evident than in the data obtained from in-situ experiments. In recent years, the experimental capability to simultaneously monitor the presence of the transforming phase (i.e. emergence of $LiFePO_4$ during discharge or $FePO_4$ during charge) through XRD during active cycling has revealed an apparent irreconcilable finding– the XRD and electrochemical data do not align in time. This has been reported by a number of researchers,[35,85,86,95,96] each observing a delay between the XRD and electrochemical data, highlighted in Figure 18 with an illustrative example. Upon the first discharge half-cycle, the collected XRD spectra remain nearly unchanged, yet according to the voltage curve electrochemical capacity is continually accessed, and only after the cell is allowed to rest does the XRD spectrum correspond to that of $LiFePO_4$. The discrepancy between the XRD and electrochemical data can be rationalized under the lens of inhomogeneous multi-particle kinetics. The voltage

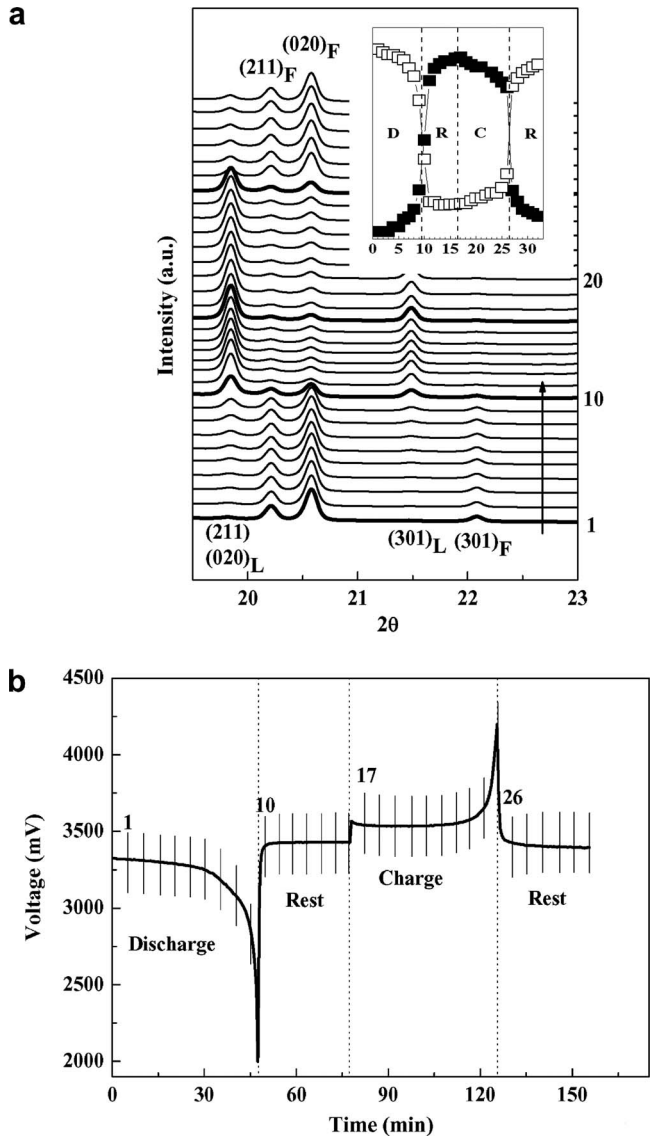

Figure 18. Experimental observation of phase-transformation delay by Chang et al.[96] (a) in-situ XRD spectra collected at 1C rate at 55°C, where L and F indicate peaks associated with $LiFePO_4$ and $FePO_4$, respectively. The simultaneously collected electrochemical data is shown in (b) with the time-points of collected XRD spectra labeled. Reprinted with permission from Ref. 96, copyright 2008, Elsevier.

measurements are collected at the electrode scale, and by virtue of the experimental setup, the XRD measurement is more local. Due to some spatial pressure variation as a result of the cell construction (specifically, pressure is relieved near the X-ray window) the XRD measurement is biased, and the $FePO_4$ in that region transforms last possibly due to poorer ionic or electronic wiring (possibly from pressure relief).[97] Moreover, Ouvrard et al. specifically note that the cell-level inhomogeneity is influenced by other parameters of the cell construction and also the cycling parameters themselves.[86]

A survey through the literature reveals that different $LiFePO_4$ electrodes (i.e. electrodes with the active mass roughly made of the same material) are capable of giving poor to excellent rate performance. Reducing the particle size to the nano-scale to improve Li transport within active particles is clearly necessary, but the remaining improvements in $LiFePO_4$ rate performance have come from electrode-scale modifications or materials modifications which improve the wiring (e.g. carbon coating and ionically conductive glass coating), as discussed earlier. This finding highlights the importance of optimizing the multi-particle kinetics to access the inherent high rate-capability of the active material. The reason the multi-particle kinetics can dictate the overall rate performance stems from the unusual shape of the single-particle potential (the thermodynamics and kinetics of which are discussed in detail in previous sections). Consequently, particles transform sequentially in the slow charging/discharging limit (described in the Multi-Particle Equilibrium section), and given no electrode-scale kinetic constraints, transform in parallel at high-rates (described in the Electrode-Scale (de)lithiation section). This highlights the importance of mitigating electrode-scale inhomogeneity, which if unaddressed ensures ineffectual rate performance due to sequentially charging particles and even worse, possible simultaneous charging and discharging of particles arising from inter-particle Li transport. The key to optimizing the electrode-scale kinetics involves electronically and ionically "wiring" each particle as close to identically as possible, meaning that transport of both Li^+ and e^- is equally unimpeded to each particle. Experimentally, this has been achieved to great success through a combination of carbon addition (through coating active particles and adding carbon in electrode assembly), coating active particles with Li^+ conducting glasses, varying the electrode thickness, and/or diluting the proportion of active material within the electrode. An effective understanding of the governing mechanism by which electrode-scale modifications enable fast charging and discharging behavior now motivates future work in improving and optimizing electrode assembly and architecture rather than focusing solely on active material synthesis.

Conclusions: Practical Implications and Future Thoughts

An ideally functioning Li-ion cathode material for large-format batteries achieves high specific and gravimetric energy density, high rate capability, long cycle life, and good safety all at low cost. Co-optimizing all of these properties is a nontrivial task, as they do not behave independently of each other. In fact, the task is challenging enough that in the thirty plus years of Li-ion battery research, only a handful of commercial cathode chemistries have emerged, and still significant improvements are required for use in applications of interest in the future (i.e. electrified vehicles). $LiFePO_4$, however, manages to perform well enough to be amongst that select group of chemistries, but it has a critical drawback– its energy density, particularly by volume, is currently considered by many too limited to be commercially feasible (~3.45 V vs. Li, ~170 mAh/g capacity) in its desired applications. Furthermore, the excellent rate performance, a hallmark of $LiFePO_4$, can only be achieved at the cost of simultaneously depleting the electrode-level energy density. First, nano-sizing active particles leads to more inefficient packing and thus lower tap density,[98–102] and second, each of incorporating carbon[103] and diluting the electrode with electrochemically inactive material,[6] lowers the volumetric energy density. Because the voltage and capacity are fixed materials properties that cannot be improved upon (short of altering the chemistry altogether), the remaining avenues of improvement lie in constructing an $LiFePO_4$ electrode that is capable of being charged and discharged at high rates without sacrificing the cell-level energy density.

An important first step toward addressing this challenge lies in identifying and understanding the kinetic mechanisms that are responsible for rapid charging and discharging in $LiFePO_4$ electrodes, which this Review has sought to piece together. To effectively and accurately model the kinetics of $LiFePO_4$ electrodes, there are three relevant length-scales that merit consideration: the $LiFePO_4$ bulk, single-particle, and multi-particle scales. Li transport within the bulk is rapid (D_{Li} ~10^{-8} to 10^{-9} cm^2/s at 300 K), and yet at the single-particle scale immobile point defects residing in the 1D diffusion path can severely impede Li migration, which to this point has only been remediated in practice by reducing the particle size to the nano-scale. Electronic conductivity is often considered to be rate-limiting in this material (σ_{e^-} ~10^{-7} to 10^{-9} S/cm[55,57]), although this Review has highlighted the need to consider coupled Li^+/e^- motion in order to correctly characterize the rate of electrochemical processes. The phase-separating

behavior of Li in the Li_xFePO_4 system not only ensures that the single-particle potential atypically does not monotonically increase with charging capacity, but also that there are several local multi-particle equilibria, each of which represents an inhomogeneous state with co-existence of fully lithiated and delithiated particles. These nuances of the system thermodynamics dictate that the (de)lithiation kinetics are equally complex– the small overpotential (~10 mV) required to access a transformation path entirely through the non-equilibrium solid solution phase facilitates not only rapid single-particle kinetics, but also accelerated transformation in those particles further along in the transformation process leading to very inhomogeneous transformation of the electrode as a whole. This framework for understanding $LiFePO_4$ has proven successful in explaining several of its "anomalous" properties observed in experiments: the weak demixing kinetics of Li_xFePO_4 solid-solutions quenched to room temperature, the lengthy time-scales required for the open-circuit voltage to equilibrate at any intermediate state of charge, the path dependence of the open-circuit voltage converging to different values at intermediate state of charge depending on charge/discharge history, the wide disparity in values of the Li diffusivity determined across different measurement techniques, the rapid single-particle kinetics despite equilibrium phase separation, and the exaggerated electrode-scale inhomogeneity readily observed in in-situ experiments.

Acknowledgments

The authors acknowledge C. Grey, A. Van der Ven, and K. Thornton for their helpful discussions and comments. This work was supported as part of the Northeastern Center for Chemical Energy Storage, an Energy Frontier Research Center funded by the U.S. Department of Energy, Office of Science, Basic Energy Sciences under Award # DE-SC0001294.

Appendices

Relation between Voltage (V) and Li Chemical Potential (μ_{Li})

The voltage V is coupled to the lithium chemical potential μ_{Li} because the number of electrons that pass through the external circuit must be identical to the number of Li^+ passing through the electrolyte. This is readily apparent when considering the entire cell at equilibrium, defined by

$$dg^{cell} = 0, \quad [A1]$$

and since the electrolyte remains unchanged before and after (dis)charge (in theory), the cell free energy g^{cell} can be separated into

$$dg^{cathode} + dg^{anode} = 0. \quad [A2]$$

At constant temperature T, the relevant formulation of the free energy is

$$(\mu_{Li}^{cathode} \cdot dn_{Li}^{cathode} + \phi^{cathode} \cdot dq^{cathode}) + (\mu_{Li}^{anode} \cdot dn_{Li}^{anode} + \phi^{anode} \cdot dq^{anode}) = 0, \quad [A3]$$

where n_{Li} refers to the number of moles of Li, Φ is electric potential, and q is electric charge. Remarking that the imposition of the electrolyte ensures that

$$dq^{cathode} = -z \cdot e \cdot dn_{Li}^{cathode} and\, dq^{anode} = -z \cdot e \cdot dn_{Li}^{anode}, \quad [A4]$$

where z is the amount of charge transported by Li^+ (i.e., z = 1) and e is the charge possessed by an electron. Rearranging the terms in A3 reveals

$$[(\mu_{Li}^{anode} - \mu_{Li}^{cathode}) - (\phi^{anode} - \phi^{cathode})]dn_{Li}^{anode} = 0. \quad [A5]$$

Therefore, under the condition of equilibrium, the difference in Li chemical potential is directly related to the difference in electrical potential between the anode and cathode (otherwise known as the voltage V):

$$\Delta\mu_{Li} = -V(in\, eV/atom). \quad [A6]$$

Li-Fe-P-O phase diagram and off-stoichiometric $LiFePO_4$

To this point strictly stoichiometric $LiFePO_4$ has been considered, yet probing the entire Li-Fe-P-O quaternary phase space sheds light not only on the stability of $LiFePO_4$ with respect to chemical decomposition, but also on which possible secondary phases are produced during synthesis given both the direction of off-stoichiometry and the oxidation environment (oxidizing to reducing conditions). Depending on their properties, secondary phases may be beneficial, neutral, or deleterious to overall electrochemical performance. In the body of literature on $LiFePO_4$, a sweeping variety of synthesis techniques have been employed, often resulting in the production of secondary phases as the consequence either of experimentally designed off-stoichiometry[7,104,105] or dopant-induced off-stoichimetry.[105,106]

From first-principles calculations, Ong et al.[92] have constructed the Li-Fe-P-O_2 phase diagram and systematically contextualized several of the experimental findings regarding secondary phase formation: Li-deficient stoichiometries have been shown to produce $Fe_7(PO_4)_6$,[106] $Fe_2P_2O_7$,[104] and iron phosphides[105] under increasingly reducing conditions; Li-rich stoichiometries tend to produce Li_3PO_4;[107] and stoichiometric $LiFePO_4$ decomposes to $Li_3Fe_2(PO_4)_3$ and Fe_2O_3 in highly oxidizing environments,[108,109] and to iron phosphides[105] under highly reducing environments. The specific tailored off-stoichiometry with iron to phosphorous deficiency ratio 2:1 (i.e. $LiFe_{1-2y}P_{1-y}O_{4-\delta}$) results in the formation of a poorly-crystallized $Li_4P_2O_7$-like secondary phase,[7] which grows to a self-selected thickness.[110] Recently, the same strategy was used to form $Li_4P_2O_7$ on $Li_3V_2(PO_4)_3$ active particles.[111]

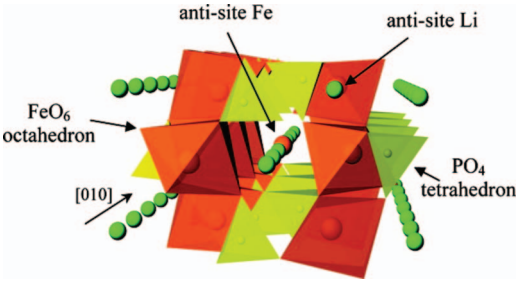

Figure A1. Illustration of $LiFePO_4$ crystal structure containing a Li–Fe anti-site defect. Reprinted with permission from Ref. 113, copyright 2008, The American Chemical Society.

Intrinsic Point Defects

Another assumption made thus far is the supposition of defect-free $LiFePO_4$. The direction of off-stoichiometry and formation energies of possible $LiFePO_4$ point defects determine whether or not there are appreciable quantities at equilibrium. First examining intrinsic defects, several computational studies[48,52,93,112,113] have cataloged the formation energy of both stoichiometric and non-stoichiometric defects for comparison against experimental observations.[114–117] The lowest energy intrinsic stoichiometric defect is the nearest neighbor Li^+–Fe^- anti-site complex,[48,52,112] where a Li^+ resides on the nearest Fe^{2+} site and vice-versa (illustrated in Figure A1), with a formation energy of ~0.515–0.55 eV[52,112] as determined from first-principles and 0.74 eV[48] when calculated with empirical potentials. Given the formation energy of the bound anti-site defect, the equilibrium concentration at common solid-state synthesis temperatures (800–1000 K) is ~0.1–0.5%, and depending on the redox environment, non-stoichiometric defects may approach comparable values.[52,112]

Chung et al.[114] observe ~1% anti-sites using aberration-corrected high-angle annular dark-field scanning transmission electron microscopy (HAADF–STEM) in $LiFePO_4$ made via solid-state synthesis. Hydrothermal synthesis can yield ~7–8% anti-sites,[118] and $LiFePO_4$ single crystals synthesized by optical floating zone method can yield ~2.5–3%.[54] All of these experimental findings inform that the number of defects in experimentally synthesized $LiFePO_4$ strays from the equilibrium concentration, likely arising due to trace quantities of impurities in precursors and employing non-equilibrium synthesis methods. Particularly telling seems to be that the low temperature synthesis methods such as hydrothermal synthesis result in the highest concentrations of defects. Furthermore, in annealing experiments by Chung et al.[114] the anti-site defect concentration decreases upon increasing the temperature, conclusively illustrating that defect concentrations are typically not near equilibrium. In the case of $LiFePO_4$ synthesized with exceedingly large quantities of point defects, not only is extensive ordering of defects observed,[119] but also the phase behavior of highly defective $LiFePO_4$ is modified with respect to Li intercalation.[120] Inferring from sloping voltage curves and in situ XRD measurements, Gibot et al.[120] observe that Li insertion proceeds through a single–phase rather than two–phase reaction in $LiFePO_4$ nanoparticles (~40 nm) with large concentrations of Fe vacancies and antisites (specifically, with composition $(\square_{0.07}Li_{0.89}Fe_{0.04})_{M1}(\square_{0.07}Fe_{0.92})_{M2}PO_4$). Likely, this occurs from defect-induced bond disorder, where the presence of distributed point defects disrupts the attractive Li^+–e^- interactions that promote phase separation, a well-observed phenomenon described in bond-disorder models.[121]

References

1. A. Padhi, K. Nanjundaswamy, and J. Goodenough, *J. Electrochem. Soc.*, **144**, 1188 (1997).
2. A. Yamada, S. Chung, and K. Hinokuma, *J. Electrochem. Soc.*, **148**, A224 (2001).
3. H. Huang, S. Yin, and L. Nazar, *Electrochem. Solid St*, **4**, A170 (2001).
4. N. Ravet et al., *J Power Sources*, **97-8**, 503 (2001).

5. S. Chung, J. Bloking, and Y. Chiang, *Nat. Mater.*, **1**, 123 (2002).
6. P. A. Johns, M. R. Roberts, Y. Wakizaka, J. H. Sanders, and J. R. Owen, *Electrochem. Commun.*, **11**, 2089 (2009).
7. B. Kang and G. Ceder, *Nature*, **458**, 190 (2009).
8. A. Yamada et al., *Nat. Mater.*, **5**, 357 (2006).
9. J. N. Reimers, *J. Electrochem. Soc.*, **139**, 2091 (1992).
10. M. M. Thackeray, P. J. Johnson, L. A. de Picciotto, P. G. Bruce, and J. B. Goodenough, *Mater. Res. Bull.*, **19**, 179 (1984).
11. T. Ohzuku and Y. Makimura, *Chemistry Letters*, **30**, 642 (2001).
12. M. Ménétrier, I. Saadoune, S. Levasseur, and C. Delmas, *J. Mater. Chem.*, **9**, 1135 (1999).
13. C. Delacourt, P. Poizot, J. Tarascon, and C. Masquelier, *Nat. Mater.*, **4**, 254 (2005).
14. J. Dodd, R. Yazami, and B. Fultz, *Electrochem. Solid St*, **9**, A151 (2006).
15. F. Zhou, T. Maxisch, and G. Ceder, *Phys. Rev. Lett.*, **97**, 155704 (2006).
16. F. Zhou, C. Marianetti, M. Cococcioni, D. Morgan, and G. Ceder, *Phys. Rev. B*, **69**, 201101 (2004).
17. B. Ellis, L. K. Perry, D. H. Ryan, and L. F. Nazar, *J. Am. Chem. Soc.*, **128**, 11416 (2006).
18. J. L. Dodd, I. Halevy, and B. Fultz, *J. Phys. Chem. C*, **111**, 1563 (2007).
19. R. Malik, F. Zhou, and G. Ceder, *Nat. Mater.*, **10**, 587 (2011).
20. L. Gu et al., *J. Am. Chem. Soc.*, **133**, 4661 (2011).
21. L. Suo et al., *Phys. Chem. Chem. Phys.*, **14**, 5363 (2012).
22. C. Delacourt, J. Rodriguez-Carvajal, B. Schmitt, J. Tarascon, and C. Masquelier, *Solid State Sci.*, **7**, 1506 (2005).
23. G. Chen, X. Song, and T. J. Richardson, *J. Electrochem. Soc.*, **154**, A627 (2007).
24. A. Van der Ven, K. Garikipati, S. Kim, and M. Wagemaker, *J. Electrochem. Soc.*, **156**, A949 (2009).
25. M. Wagemaker, F. M. Mulder, A. Van der Ven, J. Maier, and K. Kern, Editors. *Adv Mater*, **21**, 2703 (2009).
26. N. Meethong, H.-Y. S. Huang, W. C. Carter, and Y.-M. Chiang, *Electrochem. Solid St*, **10**, A134 (2007).
27. T. Maxisch and G. Ceder, *Phys Rev B*, **73**, 174112 (2006).
28. G. Chen, X. Song, and T. J. Richardson, *Electrochem. Solid St*, **9**, A295 (2006).
29. H. J. Tan, J. L. Dodd, and B. Fultz, *J. Phys. Chem. C*, **113**, 20527 (2009).
30. K. T. Lee, W. H. Kan, and L. F. Nazar, *J. Am. Chem. Soc.*, **131**, 6044 (2009).
31. W. Dreyer et al., *Nat. Mater.*, **9**, 448 (2010).
32. C. Delmas, M. Maccario, L. Croguennec, F. Le Cras, and F. Weill, *Nat. Mater.*, **7**, 665 (2008).
33. G. Brunetti et al., *Chem. Mater.*, **23**, 4515 (2011).
34. H. Matsui, T. Nakamura, Y. Kobayashi, M. Tabuchi, and Y. Yamada, *J. Power Sources*, **195**, 6879 (2010).
35. N. Meethong et al., *Chem. Mater.*, **20**, 6189 (2008).
36. A. Van der Ven and M. Wagemaker, *Electrochem. Commun.*, **11**, 881 (2009).
37. M. Takahashi, S. Tobishima, K. Takei, and Y. Sakurai, *Solid State Ionics*, **148**, 283 (2002).
38. D. Y. W. Yu et al., *J. Electrochem. Soc.*, **154**, A253 (2007).
39. P. Prosini, M. Lisi, D. Zane, and M. Pasquali, *Solid State Ionics*, **148**, 45 (2002).
40. Y. Zhu and C. Wang, *J. Phys. Chem. C*, **114**, 2830 (2010).
41. S. Franger, F. Le Cras, C. Bourbon, and H. Rouault, *Electrochem. Solid St*, **5**, A231 (2002).
42. H. Liu et al., *J. Power Sources*, **159**, 717 (2006).
43. Y.-R. Zhu et al., *Ionics*, **17**, 437 (2011).
44. M. Gaberscek, J. Moskon, B. Erjavec, R. Dominko, and J. Jamnik, *Electrochem. Solid St*, **11**, A170 (2008).
45. M. Gaberscek, R. Dominko, and J. Jamnik, *J. Power Sources*, **174**, 944 (2007).
46. M. Gaberscek, M. Kzma, and J. Jamnik, *Phys. Chem. Chem. Phys.*, **9**, 1815 (2007).
47. D. Morgan, A. Van der Ven, and G. Ceder, *Electrochem. Solid St*, **7**, A30 (2004).
48. M. Islam, D. Driscoll, C. Fisher, and P. Slater, *Chem. Mater.*, **17**, 5085 (2005).
49. S.-I. Nishimura et al., *Nat. Mater.*, **7**, 707 (2008).
50. J. Sugiyama et al., *Phys. Rev. B*, **84**, 054430 (2011).
51. C. Ouyang et al., *J. Phys.-Condens Mat.*, **16**, 2265 (2004).
52. R. Malik, D. Burch, M. Bazant, and G. Ceder, *Nano Lett.*, **10**, 4123 (2010).
53. S. Adams, *J. Solid State Electr.*, **14**, 1787 (2010).
54. R. Amin, P. Balaya, and J. Maier, *Electrochem. Solid St*, **10**, A13 (2007).
55. R. Amin, J. Maier, P. Balaya, D. P. Chen, and C. T. Lin, *Solid State Ionics*, **179**, 1683 (2008).
56. J. Li, W. Yao, S. Martin, and D. Vaknin, *Solid State Ionics*, **179**, 2016 (2008).
57. C. Delacourt et al., *J. Electrochem. Soc.*, **152**, A913 (2005).
58. C. Zhu, K. Weichert, and J. Maier, *Adv. Funct. Mater.*, **21**, 1917 (2011).
59. T. Maxisch, F. Zhou, and G. Ceder, *Phys. Rev. B*, **73**, 104301 (2006).
60. Y. Takahashi, N. Kijima, K. Tokiwa, T. Watanabe, and J. Akimoto, *J. Phys.-Condens Mat.*, **19**, 436202 (2007).
61. K. A. Seid et al., *J. Mater. Chem.*, **22**, 2641 (2012).
62. H. Tan and B. Fultz, *J. Phys. Chem. C*, **115**, 7787 (2011).
63. S. Shi et al., *Phys. Rev. B*, **68**, 195108 (2003).
64. Y. Sun, X. Lu, R. Xiao, H. Li, and X. Huang, *Chem. Mater.*, **24**, 4693 (2012).
65. A. Andersson and J. Thomas, *J. Power Sources*, **97-8**, 498 (2001).
66. N. Meethong, H.-Y. S. Huang, S. A. Speakman, W. C. Carter, and Y.-M. Chiang, *Adv. Funct. Mater.*, **17**, 1115 (2007).
67. L. Laffont et al., *Chem. Mater.*, **18**, 5520 (2006).
68. C. V. Ramana, A. Mauger, F. Gendron, C. M. Julien, and K. Zaghib, *J. Power Sources*, **187**, 555 (2009).
69. W. H. Woodford, W. C. Carter, and Y.-M. Chiang, *Energ Environ Sci.*, **5**, 8014 (2012).
70. W. H. Woodford, Y.-M. Chiang, and W. C. Carter, *J. Electrochem. Soc.*, **157**, A1052 (2010).
71. K. Weichert et al., *J. Am. Chem. Soc.*, **134**, 2988 (2012).
72. R. W. Balluffi, S. M. Allen, and W. C. Carter, *Kinetics of Materials* R. A. Kemper, Editor, 1st ed. p. 1, Wiley-Interscience, (2005).
73. D. A. Porter and K. E. Easterling, *Phase Transformations in Metals and Alloys, Third Edition (Revised Reprint)*, 2nd ed. p. 1, CRC Press, (1992).
74. J. Hong, C. Wang, and U. Kasavajjula, *J. Power Sources*, **162**, 1289 (2006).
75. J. L. Allen, T. R. Jow, and J. Wolfenstine, *J. Solid State Electr.*, **12**, 1031 (2008).
76. J. L. Allen, T. R. Jow, and J. Wolfenstine, *Chem. Mater.*, **19**, 2108 (2007).
77. G. Oyama, Y. Yamada, R.-I. Natsui, S.-I. Nishimura, and A. Yamada, *J. Phys. Chem. C*, **116**, 7306 (2012).
78. J. L. Allen, T. R. Jow, and J. Wolfenstine, *Chem. Mater.*, **24**, 1400 (2012).
79. S. Ranganathan and M. Heimendahl, *J. Mater. Sci.*, **16**, 2401 (1981).
80. M. Avrami, *J. Chem. Phys.*, **7**, 1103 (1939).
81. M. Tang et al., *Chem. Mater.*, **21**, 1557 (2009).
82. M. Tang, W. C. Carter, and Y.-M. Chiang, *Annu. Rev. Mater. Res.*, **40**, 501 (2010).
83. Y.-H. Kao et al., *Chem. Mater.*, **22**, 5845 (2010).
84. M. E. Arroyo y de Dompablo et al., *Chem. Mater.*, **22**, 994 (2010).
85. J. B. Leriche et al., *J. Electrochem. Soc.*, **157**, A606 (2010).
86. G. Ouvrard et al., *J. Power Sources*, **229**, 16 (2013).
87. P. Bai, D. A. Cogswell, and M. Z. Bazant, *Nano Lett.*, **11**, 4890 (2011).
88. R. Dominko, M. Gaberscek, A. Bele, D. Mihailovic, and J. Jamnik, *J. Eur. Ceram Soc.*, **27**, 909 (2007).
89. J. Wang and X. Sun, *Energ Environ Sci.*, **5**, 5163 (2012).
90. H. Li and H. Zhou, *Chemical Communications*, **48**, 1201 (2012).
91. M. Gaberscek, R. Dominko, and J. Jamnik, *Electrochem. Commun.*, **9**, 2778 (2007).
92. S. P. Ong, L. Wang, B. Kang, and G. Ceder, *Chem. Mater.*, **20**, 1798 (2008).
93. S. Adams and R. P. Rao, *Solid State Ionics*, **184**, 57 (2011).
94. J. Liu, M. Kunz, K. Chen, N. Tamura, and T. J. Richardson, *J. Phys. Chem. Lett.*, **1**, 2120 (2010).
95. H. C. Shin et al., *Electrochem. Commun.*, **10**, 536 (2008).
96. H.-H. Chang et al., *Electrochem. Commun.*, **10**, 335 (2008).
97. G. Ouvrard, M. Zerrouki, C. Masquelier, and M. Morcrette, *Mapping of a Battery Electrode*, (2010).
98. C. Sun, S. Rajasekhara, J. B. Goodenough, and F. Zhou, *J. Am. Chem. Soc.*, **133**, 2132 (2011).
99. H. M. Xie et al., *Adv. Mater.*, **18**, 2609 (2006).
100. L.-Q. Sun, M.-J. Li, R.-H. Cui, H.-M. Xie, and R.-S. Wang, *J. Phys. Chem. C*, **114**, 3297 (2010).
101. S. W. Oh et al., *Adv. Mater.*, **22**, 4842 (2010).
102. J. Qian, M. Zhou, Y. Cao, X. Ai, and H. Yang, *The Journal of Physical Chemistry C*, **114**, 3477 (2010).
103. Z. Chen and J. Dahn, *J. Electrochem. Soc.*, **149**, A1184 (2002).
104. P. Herle, B. Ellis, N. Coombs, and L. Nazar, *Nat. Mater.*, **3**, 147 (2004).
105. B. Ellis et al., *Faraday Discuss*, **134**, 119 (2007).
106. C. Delacourt, C. Wurm, L. Laffont, J. Leriche, and C. Masquelier, *Solid State Ionics*, **177**, 333 (2006).
107. D.-K. Kim et al., *J. Power Sources*, **159**, 237 (2006).
108. I. Belharouak, C. Johnson, and K. Amine, *Electrochem. Commun.*, **7**, 983 (2005).
109. S. Hamelet et al., *J. Mater. Chem.*, **19**, 3979 (2009).
110. A. Kayyar, H. Qian, and J. Luo, *Appl. Phys. Lett.*, **95**, 221905 (2009).
111. S. Xun, J. Chong, X. Song, G. Liu, and V. S. Battaglia, *J. Mater. Chem.*, **22**, 15775 (2012).
112. K. Hoang and M. Johannes, *Chem. Mater.*, **23**, 3003 (2011).
113. C. A. J. Fisher, V. M. H. Prieto, and M. S. Islam, *Chem. Mater.*, **20**, 5907 (2008).
114. S.-Y. Chung, S.-Y. Choi, T. Yamamoto, and Y. Ikuhara, *Phys. Rev. Lett.*, **100**, 125502 (2008).
115. S.-Y. Chung, S.-Y. Choi, T. Yamamoto, and Y. Ikuhara, *Angew Chem. Int. Edit.*, **48**, 543 (2009).
116. K. Jensen, M. Christensen, C. Tyrsted, and B. B. Iversen, *J. Appl. Crystallogr*, **44**, 287 (2011).
117. J. Chen and J. Graetz, *Acs Appl. Mater. Inter.*, **3**, 1380 (2011).
118. S. Yang, Y. Song, P. Zavalij, and M. Whittingham, *Electrochem. Commun.*, **4**, 239 (2002).
119. S. Hamelet et al., *Chem. Mater.*, **23**, 32 (2011).
120. P. Gibot et al., *Nat. Mater.*, **7**, 741 (2008).
121. A. N. Berker, *J. Appl. Phys.*, **70**, 5941 (1991).
122. V. Srinivasan and J. Newman, *J. Electrochem. Soc.*, **151**, A1517 (2004).